Mechanisms of interannual variability of deep convection in the Greenland Sea

Article

Accepted Version

Bashmachnikov, I. L., Fedorov, A. M., Golubkin, P. A., Vesman, A. V., Selyuzhenok, V. V., Gnatiuk, N. V., Gnatiuk, L. P., Hodges, K. I. ORCID: https://orcid.org/0000-0003-0894-229X and Dukhovskoy, D. S. (2021) Mechanisms of interannual variability of deep convection in the Greenland Sea. Deep Sea Research Part I: Oceanographic Research Papers, 174. 103557. ISSN 0967-0637 doi: 10.1016/j.dsr.2021.103557 Available at https://centaur.reading.ac.uk/97608/

To link to this article DOI: http://dx.doi.org/10.1016/j.dsr.2021.103557

Publisher: Elsevier

Mechanisms of Interannual Variability of Deep Convection in the Greenland Sea

Igor L. Bashmachnikov[1,2], Aleksandr M. Fedorov[1,2,3], Pavel A. Golubkin[2], Anna V. Vesman[1,2,3], Valeria V. Selyuzhenok[1,2], Natalia V. Gnatiuk[2], Leonid P. Bobylev[2], Kevin I. Hodges[4], Dmitry S. Dukhovskoy[5]

[1]St. Petersburg State University, SPbSU, 7/9 Universitetskaya nab., St. Petersburg, 199034, Russia
[2]Nansen International Environmental and Remote Sensing Centre, 14 Line V.O., 7, St.Petersburg, 199034, Russia
[3]Arctic and Antarctic Research Institute, Bering str., 38, St.Petersburg, 199397, Russia
[4]Department of Meteorology, University of Reading, Reading, United Kingdom
[5]Florida State University, Tallahassee, Florida, USA.

Corresponding author: i.bashmachnikov@spbu.ru

Highlights

- The upper ocean salinity governs the interannual change of the convection intensity
- Interannual change of the upper ocean advection is of the primarily importance
- Interannual change of the sea ice melt is of the secondary importance
- The ocean-atmosphere heat release is only of the tertiary importance

Keywords

deep convection, the Greenland Sea, oceanic freshwater advection, winter ice conditions

Acknowledgments

The research was funded by the Saint Petersburg State University (project N 75295423). D.S. Dukhovskoy was funded by the DOE (award DE-SC0014378).

Abstract

This study investigates the physical processes and mechanisms driving the interannual variability of deep convective intensity in the Greenland Sea from 1993 to 2016. The intensity of deep convection is derived using the traditional Maximum Mixed Layer Depth, the total surface area with the monthly-mean mixed layer depth exceeding 800 m and various indices. All metrics show that the intensity of convection increased during the 2000s.

The analysis demonstrates that observed increases of the deep convective intensity in the Greenland Sea is associated with an increase in the upper ocean salinity. The long-term interannual variability of deep convection is mainly linked to the variation of the water salinity during the preceding summer and the current winter. In turn, the variability of the upper-ocean salinity is primarily related to the variability in the advection of Atlantic water into the region with the re-circulating branches of the West Spitsbergen Current and to a lesser degree, to the local sea ice melt. For only two winters during the study period did the sea ice contribute significantly to a weakening of the intensity of deep convection by substantially reducing oceanic heat loss to the atmosphere. The variability in the advected heat is effectively abated by the concurrent variations of oceanic heat release to the atmosphere. The interplay between the interannual variability of the oceanic heat advection and the winter air-sea net heat flux leads to a noticeable reduction of the interannual variability of both fluxes over the convective regions. As a result, the direct effect of the varying air-sea heat exchange did not have a

pronounced direct effect on the interannual variation in the intensity of deep convection in the Greenland Sea, at least during the study period.

1. Introduction

In this paper, we investigate the mechanisms driving the interannual variability of the intensity of Deep Convection (DC) in the Greenland Sea. The process of deep convection is affected by a number of linked and interacting processes. However, the leading mechanisms governing the interannual variability of deep convection in the region remain a subject of discussion. We show that the oceanic heat release to the atmosphere is of secondary importance for the long-term interannual variability of the DC. This is due to the relatively small interannual variability of the heat flux compared to other factors. The intensity of DC during the study period (1993-2016) was found to be primarily controlled by the long-term variations in the volume transport and the thermohaline characteristics of the Re-circulating Atlantic Water (RAW) reaching the central Greenland Sea. This acts together with a possible positive feedback mechanism between the Atlantic Meridional Overturning Circulation (AMOC) and the deep convection that may govern the system on interdecadal or longer time scales (Stommel et al., 1958; Levermann and Born, 2007).

1.1 Deep convection in the Greenland Sea and its variability

The AMOC is an essential component of the global conveyor belt (Lappo, 1984; Broecker, 1987, 1991), as well as of the global climate system. The AMOC links the circulation in the Atlantic and the Southern oceans in a unified system of two semi-closed interacting multilevel circulation cells (Lumpkin and Speer, 2007; Garzoli and Matano, 2011; Johnson et al., 2019). The observed faster change of the surface air temperature in polar regions (Gulev et al., 2008; Johannessen et al., 2016) is argued to be associated with the AMOC intensity (Lockwood, 2001; Drijfhout, 2015). The atmospheric conditions, as well as the direct oceanic advection to the subpolar and polar regions affects the DC (Buckley and Marshall, 2016; Gladyshev et al., 2016; Lozier et al., 2019). In turn, among other factors, the variability of the DC in the North Atlantic, linking its upper and deep branches of its upper circulation cell and assuring its continuity, is considered to be one of the mechanisms forcing the AMOC variability (Buckley and Marshall, 2016; Johnson et al., 2019; Volkov et al., 2020).

We define DC as the vertical mixing of water driven by gravitational instability that results in a renewal of intermediate and/or deep water masses participating in the formation of the deep branch of the AMOC. In the Greenland Sea, such water masses are the Greenland Sea Intermediate Water (the typical depth range is 500-1000 m) with a temperature of -0.44 ~ -0.8 ^{o}C and a salinity around 34.90 and the Greenland Sea Deep Water (below 1000 m) with a temperature of -0.8 ~ -1.2 ^{o}C and a salinity ~34.90 (Nagurny and Popov 1985; Alekseev et al., 1989; Moretsky and Popov, 1989; Johannessen et al., 1991, 2005; Korablev, 2001). Both water masses are formed as a mixture of the Re-circulating Atlantic Water with the Arctic Intermediate and Deep water, regularly modified during winter convection events (Rudels et al., 2002; Jeansson et al., 2008; Langehaug and Falck, 2012).

The DC in the Greenland Sea has been extensively studied during several comprehensive international projects since the 1980s (see reviews by Killworth, 1983; GSP Group 1990; Chu and Gascard, 1991; Marshall and Schott, 1999). A series of field experiments (GSP Group in 1990; Drange et al., 2005; Bashmachnikov et al., 2018) and theoretical models (Chu and

Gascard, 1991; Visbeck et al., 1996; Marshall and Schott, 1999; Kovalevsky et al., 2020) have revealed typical patterns of evolution of the areas of DC.

DC "chimneys" represent deeply mixed regions (often reaching 1500- 2000 m depth) which are relatively small in diameter (typically of 20-50 km), each composed of a number of high-density negatively buoyant DC plumes (GSP Group, 1990; Johannessen et al., 1991; Kovalevsky 2002; Yashayaev et al., 2007). The latter structures have typical horizontal scales of order of 100 m (Marshall and Schott, 1999; Johannessen et al., 2005). The sea-level and the water density gradients turn the chimneys into mesoscale heton structures, with cyclonic circulation in the upper ocean and anticyclonic circulation at depth (Marshall and Schott, 1999; Kovalevsky, 2002). The resulting potential vorticity anomalies inhibit fluid exchange across the boundaries of the structure, adding stability to the chimneys.

A stable DC chimney is a result of the balance between the ocean buoyancy release to the atmosphere and the horizontal turbulent buoyancy exchange through the side-walls of the DC region. The latter is a result of the dynamic instability developed along the "walls" of the chimney, which leads to the water exchange with sub-mesoscale eddies (Chu and Gascard, 1991; Jones and Marshall, 1993). The eddy-like structures with radii 7-15 km, which are of the order of the first baroclinic Rossby deformation radius (Nurser and Bacon, 2014), have previously been detected at the boundary of a DC region in the Boreas basin of the Greenland Sea (Johannessen et al., 2005).

The dynamical processes regulating the vertical and horizontal buoyancy fluxes in DC regions, range from sub-mesoscale to mesoscale. Only very high resolutions (less than 1 km) non-hydrostatic hydrodynamic models are able to reproduce the approximate dynamics of physical processes during formation and decay of a DC chimney (Jones and Marshall, 1993; Paluszkiewicz and Romea, 1997; Androsov et al., 2005; Kovalevsky et al., 2020). Even in eddy-resolving models with the spatial resolution of 2-4 km, the DC dynamics are parameterized (Dukhovskoy et al., 2019). Depending on the parameterization used in a model the DC intensity can vary within wide limits (Timmerman et al., 2004). The analysis of in situ observations remains critical for progress to be made in further understanding and modelling this climatically important phenomenon.

1.2 Factors governing interannual variability of DC in the Greenland Sea

In spite of the fact that a number of mechanisms controlling DC intensity in the subpolar North Atlantic have been suggested (Glessmer et al., 2014; Moore et al., 2015; Boning et al., 2016; Luo et al., 2016; Yang et al., 2016), the principal factors driving the observed interannual variability of the DC intensity remain unclear. It is generally accepted that the intensity of DC is a function of the air-sea heat and freshwater fluxes and stratification of the upper water column at the beginning of the convective event (Visbeck et al., 1996). Factors controlling interannual and interdecadal variability of DC in the Greenland Sea discussed in previous studies can be divided into three major groups:

1) the air-sea buoyancy (heat and/or freshwater) fluxes,

2) the buoyancy variability due to oceanic heat and/or freshwater advection,

3) the intensity of the cyclonic circulation in the central Greenland Sea.

These factors are reviewed in the following sections.

The variability in the upper ocean stratification is mostly governed by changes in the upper ocean temperature and salinity, as the thermohaline characteristics of the deep layers vary at significantly smaller amplitudes and over longer time scales. The Upper Greenland Sea water is observed in the upper 200-500 m layer. Its temperature typically varies from 0 to 3 ^{o}C and salinity – from 34.4 to 34.9. Most of the results suggest that in the central part of the Greenland Sea, the sea-surface salinity declined in the late 1970s and did not recover until the end of the 1990s (Johannessen et al., 1991; Alekseev et al., 2001; Glessmer et al., 2014). There are indications that this tendency has reversed since the beginning of the 2000s (Yashayaev and Seidov, 2015; Dukhovskoy et al., 2016; Lauvset et al., 2018). A tendency for warming of the Greenland Sea at all depths has also been noted (Lauvset et al., 2018; Selyuzhenok et al., 2020).

1.2.1. Heat and freshwater fluxes through the sea surface

Since the work of Nansen (1912), the ocean-atmosphere buoyancy flux has been considered the principal reason for triggering DC development in the subpolar seas (Marshall and Schott, 1999; Bailey et al., 2005; Falina and Safronov, 2015; Yang et al., 2016). The typical sea-surface heat loss in the central Greenland Sea of 120-160 W m^{-2} leads to a moderate convective deepening, while its episodic increase to greater than 200 W m^{-2} may lead to a substantial increase in the deepening rate and a formation of a deep chimney within a week (Moore et al., 2015; Kovalevsky et al., 2020). In particular, the magnitude of the air-sea fluxes may drastically increase when atmospheric cyclones are crossing the region (Zolina and Gulev, 2003; Dickson et al., 2008; Skagseth et al., 2008; Tilinina et al., 2016; Dukhovskoy et al., 2017). Thus, variations in the cyclonic activity should also be considered as a factor contributing to the interannual variability of the DC intensity.

Sea ice cover affects the intensity of DC by hampering the heat and freshwater exchange with the atmosphere. It has been seen that, with sea ice extending into the central Greenland Sea, DC does not occur (Mysak et al., 1990; Moore et al., 2015; Vage et al., 2018). On the other hand, formation of sea ice might trigger haline convection through brine rejection (Meincke et al., 1997). The sea ice retreat observed during 1980 through 2015 is believed to have induced the winter air warming over the Greenland Sea, which resulted in a decrease of the ocean-atmosphere heat release by 20% and limited DC (Moore et al., 2015; Vage et al., 2018). The reliability of the these hypotheses remains unproven because observations demonstrating the link between long-term variability of the ice area and the DC intensity is absent. As over 65% of the sea-ice of the Greenland Sea is imported from the Arctic (Mironov, 2004), the inter-annual variability of the ice extent in the Greenland Sea is also linked to ice dynamics in the Arctic and to the atmospheric circulation over the Fram Strait (Vinje and Finnekasa, 1986; Gudkovich and Nikolaev, 2001; Koenigk et al., 2007; Giles et al., 2012; Kohl and Serra, 2014).

The interannual variability of the net precipitation over the Greenland Sea is not the primary source of the interannual variability of the freshwater content of the upper Greenland Sea (Peterson et al., 2006). While the major influence of the sea ice and freshwater advected from the Arctic Ocean is attributed to the western Greenland Sea (see Supplement 7.4), net precipitation directly affects its central areas (DC sites). Net precipitation decreased during the 1990s-2000s, linked to changes in the North Atlantic and Arctic Oscillations, when both indices shifted from being mostly positive to a mostly negative phase (Peterson et al., 2006).

1.2.2. Horizontal buoyancy fluxes

The Upper Greenland Sea water is the mixture of the Polar Water (with temperature below zero and salinity from 33 to 34) exported from the Arctic Ocean and the Re-circulating Atlantic Water (with temperature over 3 ^{o}C and salinity around 34.9) originating from the West

Spitsbergen Current (WSC) in the eastern Fram Strait (Rudels et al., 2002; Jeansson et al., 2008). The water then joins the East Greenland Current (EGC) and enters the central Greenland Sea through re-circulation patterns (Fig. 1). Several studies have speculated that freshening events in the upper Greenland Sea in the 1960s, the early 1980s and the late 1990s were due to an increased influence of the Polar Water, whereas salinity variations in the 1970s and from the late 1980s to the early 1990s were due to the stronger RAW influence (Johannessen et al. 1991; Alekseev et al., 2001; Glessmer et al., 2014). The detected 2-3-year and 6-7-year periodicities in the upper ocean salinity correspond to the same periodicities in the oceanic meridional heat fluxes into the region (Dukhovskoy et al., 2004; Proshutinsky et al., 2015; Bashmachnikov et al., 2016a).

The Polar water from the Arctic Ocean forms approximately half of the freshwater storage in the Nordic Seas (Peterson et al., 2006). The volumes of liquid freshwater and ice transported through the Fram Strait are of the same order of magnitude (Vinie, 1986; Serreze et al., 2006; Maslowski et al., 2008; Rabe et al., 2013; Glessmer et al., 2014). Both fluxes have increased in recent decades (Kwok, 2004; Selyuzhenok et al., 2020). However, most of this freshwater passes through the Greenland Sea, following its continental margin (Curry et al., 2005; Peterson et al., 2006; Serreze et al., 2006; Koenigk et al., 2007; Boning et al., 2016). Only a small portion of the freshwater becomes trapped by the re-circulation along the Jan Mayen ridge (Björk et al., 2001; Peterson et al., 2006; Dukhovskoy et al., 2019). Winds and eddies may episodically transport the freshwater and ice in the central areas (Johannessen et al., 1987; Gascard et al., 2002; Gerdes et al., 2005; Koenigk et al., 2008; Proshutinsky et al., 2015; von Appen et al., 2018), but it is not known whether these fluxes are of any significance.

Over the past 20 years, the freshwater discharge from the Greenland Ice Sheet has increased by 50%. The surplus of freshwater discharge forms about half of the freshwater volume fluxed into the North Atlantic during the Great salinity anomaly of the 1970s (Box et al., 2004; Bamber et al., 2012; Swingedouw et al., 2014; Lenaerts et al., 2015; Boning et al., 2016). On the other hand, model results suggest that Greenland meltwater does not leave the northeast Greenland shelf therefore having a very small direct influence on the convective areas in the central Greenland Sea (Dukhovskoy et al., 2019).

The relatively warm and salty Atlantic water, re-circulating in the southern Fram Strait, can strongly influence the buoyancy of the upper Greenland Sea (Johannessen et al., 1991; Alekseev et al., 2001; Furevik et al., 2002; Yashayaev, 2007; Dickson et al., 2008; Beszczynska- Möller et al., 2012; Marnela et al., 2013; Glessmer et al., 2014; Deshayes et al., 2014; Yang et al., 2016; Boning et al., 2016; Luo et al., 2016; Lauvset et al., 2018; Ferreira et al., 2018). Strongly modified in the Fram Strait by mixing with the Polar Water and with the modified Atlantic Water returning from the Arctic (Langehaug and Falck, 2012), the long-term variations in RAW properties conserve the original anomalies of the Atlantic water in the Faroe-Shetland Channel (Lauvset et al., 2018). According to some estimates, the RAW forms up to 90% of the upper ocean water in the central Greenland Sea, while only 1-2% is formed by the Arctic Polar water (Johannessen et al., 1991; Alekseev et al., 2001; Marnela et al., 2013). Although the interannual variability along the Atlantic Water pathway shows clear differences linked to various atmospheric forcing mechanisms (Lien et al., 2013; Chafik et al., 2015; Raj et al., 2018; Vesman et al., 2020), since the 1990s the Atlantic Water inflow shows a clear decadal tendency to increase along the whole pathway from the Faroe-Shetland Channel to the Fram Strait (Lumpkin, Speer, 2007; Schauer et al., 2008; Hakkinen, Rhines, 2009; Piechura, Walczowski, 2009; Srokosz et al., 2012; Beszczynska-Möller et al., 2012; Walkzowski, 2014; Yashayaev, Seidov 2015; Lauvset et al., 2018). Consistently, observations from the recent decades show that, despite some increase in the freshwater flux from the Arctic, the upper layer salinity has been increasing in the central Greenland Sea (Dickson et al., 2008; Dukhovskoy et al., 2016, Lauvset et al., 2018; Selyuzhenok et al., 2020), suggesting lower stratification and favouring a stronger DC. The weaker haline stratification might yet be partly mitigated by an observed increase of the temperature of the Atlantic Water at the end of the 1990s (Johannessen et al., 1991; Alekseev et al., 2001; Dickson et al., 2008).

1.2.3. Intensity of cyclonic circulation

The cyclonic circulation in the Greenland Sea (Greenland Gyre) causes Ekman pumping that brings dense weakly stratified water closer to the surface and results in a doming of isopycnals in the central Greenland Sea (Rossby et al., 2009). This decreases the depth-integrated heat and freshwater content above the weakly stratified mid-depth ocean and facilitates development of DC during winter. Therefore, the intensity of the Greenland Gyre might be another factor controlling the variability of DC in the Greenland Sea (Clarke and Gascard, 1983; Jonsson, 1991; Meincke et al., 1992; Malmberg and Jonsson, 1997; Marshall and Schott, 1999).

In summary, Sections 1.2.1-1.2.3 show that previous studies have presented a number of plausible, sometimes contradictory, hypotheses explaining some of the variability of DC in the Greenland Sea. In this paper, we employ observational-based hydrographic data-sets to perform a comprehensive analysis of the most plausible mechanisms affecting the intensity of DC during the period covering an intense observational effort in the region, from 1993 to 2016. We will show that the buoyancy input due to horizontal advection plays the principal role in the interannual variability of DC, whereas the air-sea fluxes and the variability of the sea-ice extent are of secondary importance.

2. The data-sets

2.1 Oceanic data

To compute the current velocity and the mean relative vorticity, the AVISO14 altimetry data-set is used (https://www.aviso.altimetry.fr/en/my-aviso.html). The data are available since 1993 with a horizontal resolution of 0.25^{o}x0.25^o (28 km x 7 km in the central Greenland Sea). The current velocity and relative vorticity are computed from the sea-level data using the 7-point stencil width formulae to minimize the noise level (Arbic et al 2012).

The 3D fields of water density and ocean currents are obtained from the ARMOR3D data-set, a relatively new global ocean state product combining in situ and satellite ocean observations. The data are available since 1993, limited to the beginning of the satellite altimetry (Rosmorduc and Hernandez, 2003; Muller et al., 2019). A relatively robust estimate of oceanic advective fluxes is possible since 1993, as well.

In ARMOR3D, "synthetic" temperature and salinity at different water levels are first derived from altimeter and sea surface temperature (SST) anomalies through a multiple regression (Guinehut et al., 2004). The regression coefficients are regionally obtained by combining the satellite and all available sub-satellite historical data. The synthetic thermohaline fields are combined with in situ historical data in the optimal interpolation procedure to obtain the final product (Guinehut et al., 2012). Geostrophic currents are then computed by extrapolating the sea surface altimetry currents downwards, using the thermal wind equations (Mullet et al. 2012). As a result, the ARMOR3D data-set contains monthly 3D fields of temperature, salinity, and geostrophic currents, gridded to the standard depth levels with 0.25°×0.25° spatial resolution (Verbrugge et al. 2017). The use of satellite information results in more robust thermohaline and current velocity fields, available with a higher spatial and temporal resolution then the results of interpolation of in situ data only (Larnicol et al., 2006). The stated maximum RMS error is 0.3°C in temperature and 0.02 in salinity in the upper 100-m layer (Verbrugge et al. 2017). Below 1500 m, the data-set is replaced with the WOA13 climatology modified by available in situ profiles. This makes values of interannual variability of temperature and salinity profiles below 1500 m less reliable. Comparison of the interannual variability of the DC intensity derived from ARMOR3D with that from the GLORYS reanalysis shows a high correlation between the results (see Supplement 7.2). We also develop alternative metrics, which do not use these deep levels (see Section 3.2)

To verify the volume and heat fluxes derived from ARMOR3D in the Greenland Sea, independent data from moorings deployed in the southern Fram Strait along 77.8°N (Beszczynska-Möller et al., 2012; Beszczynska-Möller, 2015) are used. The data set consists of the temperature, salinity, and current velocity information at 10 moorings from 1997 to 2011 (PANGAEA: https://doi.pangaea.de/10.1594/PANGAEA.845938). In addition, pre-computed oceanic heat fluxes from the Hornbanki mooring in the northern Denmark Strait (the NACLIM project, Jonsson and Valdimarsson, 2012) are also used. The comparison shows that ARMOR3D reproduces the main seasonal cycle, as well as the interannual variability, with sufficient accuracy in spite of a somewhat lower interannual variability (Vesman et al., 2020). In areas with frequent ice cover and with increasing depth, the accuracy of the ARMOR3D heat fluxes decrease. Nevertheless, ARMOR3D reproduces well the interannual variability of heat and freshwater fluxes in the upper 500-m layer, which encompasses the main core of the Atlantic water re-circulation in the Greenland Sea (Rudels et al., 2002; Jeansson et al., 2008).

2.2 Atmospheric data

The ocean-atmospheric freshwater and heat exchange are computed from the 6-hourly ERA-Interim reanalysis data (Dee et al., 2011) on a 0.75°×0.75° grid (https://apps.ecmwf.int/datasets/data/interim-full-daily/levtype=sfc/), obtained from the European Centre for Medium-range Weather Forecasts (ECMWF). Reanalysis wind speed, air and sea surface temperatures, relative humidity, and surface pressure fields are used for surface turbulent flux calculation employing the COARE 3.5 algorithm (Fairall et al., 2003). The results are further averaged to the monthly means.

Sea-surface net solar radiation derived from ERA-Interim reanalysis data represents the sum of the shortwave (solar, direct and diffuse) radiation (https://apps.ecmwf.int/codes/grib/param-db?id=176) and net longwave (downwards minus upwards) radiation (https://apps.ecmwf.int/codes/grib/param-db?id=177).

2.3. Ice data

The variability of the ice volume in the Greenland Sea is derived from the PIOMAS reanalysis. The reanalysis is based on the Parallel Ocean Program model coupled with a thickness and enthalpy distribution (TED) sea ice model. The reanalysis assimilates NSIDC near-real time satellite passive microwave sea ice concentrations and NCEP/NCAR sea surface temperature in the ice-free areas (Zhang and Rothrock, 2003). Validation of the PIOMAS sea-ice thickness with in situ, submarine, and satellite observations for the Arctic suggests that the PIOMAS uncertainty in the monthly mean sea-ice thickness is below 80 cm (Schweiger et al., 2011). Similar to the Arctic Ocean, the model tends to overestimate thickness of thin ice and underestimate thickness of thick ice in the Greenland Sea (Selyuzhenok et al., 2020). However, deduced from PIMAS the interannual variability of the ice volume flux through the Fram Strait and the interannual ice volume variation integrated over the Greenland Sea show high correlations with independent in situ and satellite-derived Cryosat observations (Selyuzhenok et al., 2020).

In this study, monthly mean Greenland freshwater discharge rates include solid (ice) discharge, tundra runoff and the ice sheet meltwater in Greenland Sea (between the Fram Strait and 73^{o}N) (https://www.bodc.ac.uk/data/published_data_library/catalogue/10.5285/643aa9bc-bcd6-45ad-e053-6c86abc07da0/, Bamber et al, 2018). Approximately half of the freshwater flux integrated along the eastern Greenland coast enters the Greenland shelf, onshore of the study region shown in Figure 1(a) (Dukhovskoy et al. 2016, 2019).

3. Methods

All notations used throughout the text are summarised in Supplement 7.1

3.1 Variability of the mixed layer depth in the Greenland Sea

The interannual variation of the DC intensity is typically obtained as the maximum mixed layer depth (*MMLD**). Hydrographic ship observations reveal notable interannual variability in the maximum MLD in the Greenland Sea (Table 1 and Fig. 1).

Table 1. Interannual variability of the maximum MLD (m) in the Greenland Sea. The range of values of the *MMLD** come from different sources.

year	*MMLD** (m)	Reference
1970/71	3500	Malmberg, 1983
1981/82	500	Clarke et al., 1990
1983/84	3500	Nagurny and Popov, 1985
1986/87	200	GSP-Group, 1990; Fischer et al., 1995; Lauvset et al., 2018; Somavilla, 2019; Brakstad et al., 2019
1987/88	1300	GSP-Group, 1990; Fischer et al., 1995
1988/89	1400-2000	GSP-Group, 1990; Fischer et al., 1995
1989/90	550	Somavilla, 2019
1990/91	500	Somavilla, 2019
1991/92	550	Somavilla, 2019
1992/93	800-1000	Fischer et al., 1995; Buderus et al., 1998; Lauvset et al., 2018; Brakstad et al., 2019
1993/94	700	Fischer et al., 1995; Buderus et al., 1998; Lauvset et al., 2018; Brakstad et al., 2019
1994/95	>1000	Fischer et al., 1995; Buderus et al., 1998; Lauvset et al., 2018; Brakstad et al., 2019
1995/96	>1000	Fischer et al., 1995; Buderus et al., 1998; Brakstad et al., 2019

1996/97	700	Somavilla, 2019
1997/98	550	Somavilla, 2019
1998/99	500	Somavilla, 2019
1999/00	900	Somavilla, 2019
2000/01	1500	Lauvset et al., 2018; Brakstad et al., 2019
2001/02	1500	Lauvset et al., 2018; Brakstad et al., 2019
2002/03	1600	Latarius and Quadfase, 2016
2003/04	1300	Somavilla, 2019
2004/05	1350	Somavilla, 2019
2005/06	500-800	Latarius and Quadfase, 2016; Lauvset et al., 2018; Somavilla, 2019; Brakstad et al., 2019
2006/07	1000	Latarius and Quadfase, 2016; Lauvset et al., 2018; Brakstad et al., 2019
2007/08	1500	Lauvset et al., 2018; Somavilla, 2019; Brakstad et al., 2019
2008/09	1500	Latarius and Quadfase, 2016
2009/10	500-1400	Latarius and Quadfase, 2016; Lauvset et al., 2018; Somavilla, 2019; Brakstad et al., 2019
2010/11	1500	Lauvset et al., 2018; Brakstad et al., 2019
2011/12	1600	Latarius and Quadfase, 2016
2012/13/	1600	Lauvset et al., 2018; Brakstad et al., 2019
2013/14	100	Lauvset et al., 2018; Brakstad et al., 2019
2014/15	800	Lauvset et al., 2018; Brakstad et al., 2019

It is noteworthy that for the same years, various authors give different maximum winter MLD. This stems from the limited spatial and temporal coverage of in situ observations analysed in the previous studies, as well as from inconsistencies in the definition of the MLD and the different methodologies for the MLD detection. This is discussed in more detail in the following sections.

Analysis of ARMOR3D hydrographic fields and individual vertical profiles (from EN4 Hadley Center data-set, https://www.metoffice.gov.uk/hadobs/en4/) show that at any point in the central Greenland Sea the DC may exceed 1000 m, at least once during the last two decades (Fedorov et al., 2018; Bashmachnikov et al., 2018). However, the most frequent DC is localized in a limited region of the central Greenland Basin (Fig. 1a). Strong DC in other regions is relatively rare. Thus, in the Boreas basin, DC was observed to penetrate down to 2000 m (Johannessen et al., 1991, 2005), but much less frequently then in the Greenland basin (Fig. 1, Fedorov et al., 2018; Bashmachnikov et al., 2018).

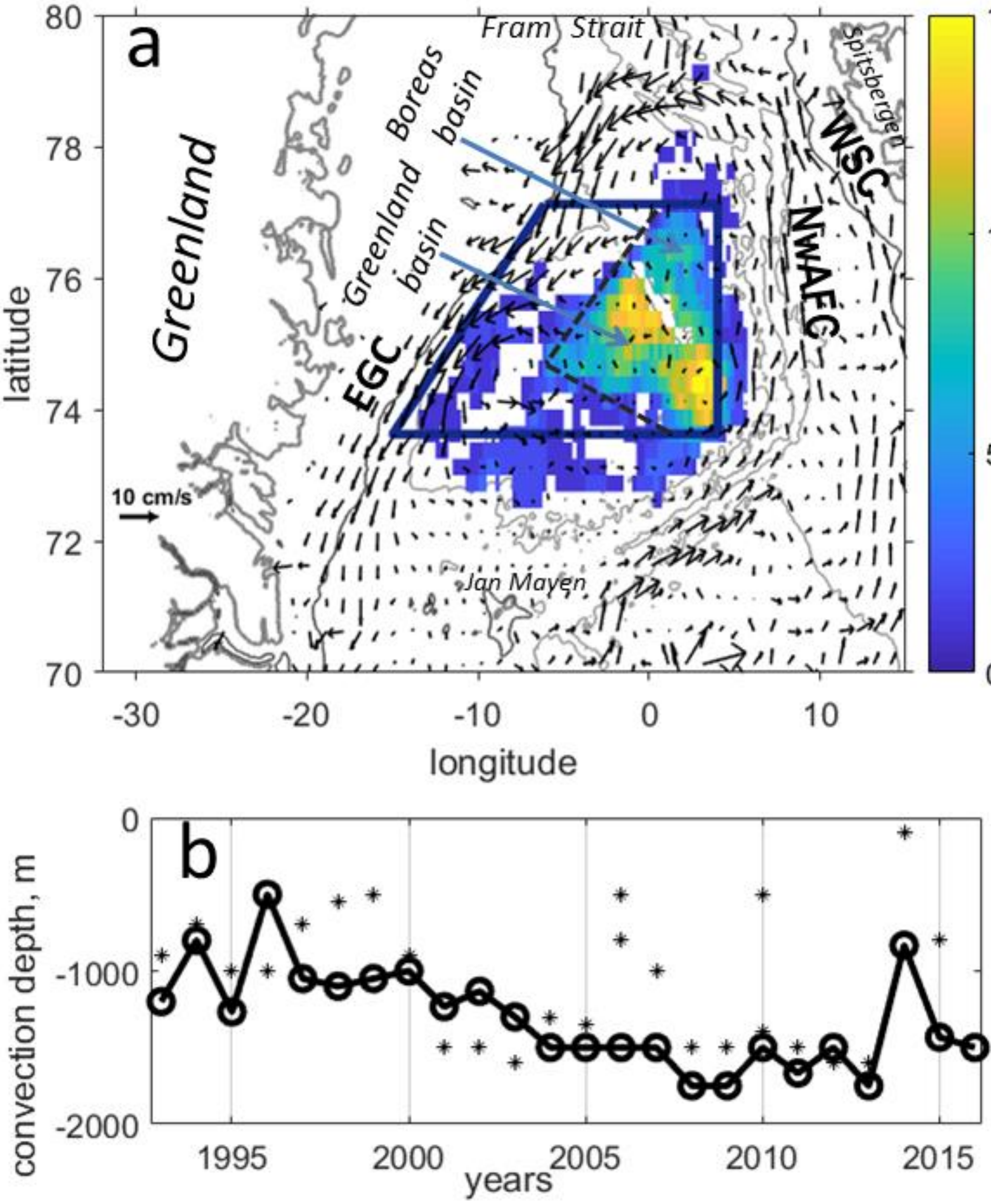

Fig. 1. (a). The study region. Colour represents the number of winter months (January to April of 1993-2016) in a grid-point with MLD over 1000 m divided by the total number of winter months; derived from ARMOR3D data-set (see Bashmachnikov et al., 2018). Vectors are the mean currents derived from AVISO altimetry. The region of deep convection is contoured with the dark-blue line designating the study domain discussed in the text; the region with the most frequent deep convection is limited by the dashed blue line from the west. Grey lines mark 500 m and 2500 m isobaths. EGC is the East Greenland Current, NwAFC is the Norwegian Atlantic Front Current, WSC is the West Spitsbergen Current. (b) Maximum winter convection depth (MMLD, m), derived from ARMOR3D data-set (line with empty circles) and from various literature sources (Table 1, stars).*

3.2 Estimation of the intensity of DC

For the calculation of MLD, the small-scale noise is removed using a moving average filter on the ARMOR3D vertical profiles with a 10-m window. Only profiles over the deep Greenland

Sea (with water depth exceeding 800 m) are considered. The gravitationally unstable segments of the profiles are artificially mixed until neutral stratification is achieved at all levels. If the artificially mixed layer exceeds half the local ocean depth, the profile is excluded as unreliable.

The MLD is detected using three different algorithms previously used by de Boyer Montegut et al. (2004), Kara et al. (2000), and Dukhovskoy (first presented in Bashmachnikov et al., 2018). The method of de Boyer Montegut et al. (2004) detects MLD as the upper level, where the potential density difference ($\Delta\sigma$) between the tested and the fixed near sea surface level (z_b=10 m) exceeds a pre-defined critical value ($\Delta\sigma_c$): $\Delta\sigma > \Delta\sigma_c$. Tests of the algorithm performance shows $\Delta\sigma_c$ = 0.01 kg m^{-3} to be optimal for the Greenland Sea. The algorithm of Kara et al. (2000) is similar, except that the critical temperature difference ΔT_c is now fixed. The density difference is derived from the equation of state using temperature at the upper level z_b, $T(z_b)$, while salinity is fixed to $S(z_b)$. Due to the nonlinearity of the equation of state, for a lower $T(z_b)$, we get smaller $\Delta\sigma_c$ for the same ΔT_c and a fixed salinity, which allows a more accurate detection of the MLD in smoother winter density profiles compared to de Boyer Montegut et al. (2004). Tests showed ΔT_c = 0.1 °C to be optimal for the study region. Dukhovskoy suggests fixing MLD at the uppermost level where the vertical density gradient exceeds its local standard deviation (within the ±50 m window). This algorithm does not depend on a pre-defined critical value and takes into account the intensity of the vertical density variations in each profile. This algorithm is sensitive to changes in the vertical density gradients, which characterizes the transition from the upper mixed layer to the pycnocline. As the upper "mixed" layer of the measured vertical profiles is often not completely homogeneous in the real ocean, this method provides a good balance between avoiding false detection of the MLD at relatively small density fluctuations within the MLD and the ability to detect even a weak pycnocline at large depths, which is often missed by the $\Delta\sigma_c$ threshold methods. A similar methodology has been used by Pickart et al. (2002), but applied to vertical variations of density instead of variations of density gradients. Analysis shows that, in most cases, the results obtained by the three algorithms are similar (Fedorov et al., 2018; Bashmachnikov et al., 2018). However, the method of Dukhovskoy, is more accurate and robust, in particular for a weak pycnocline. It is selected as the principle method used in this study.

Due to the small area of the chimneys (Marshall and Scott, 1999; Johannessen et al., 1991, 2005; Wadhams et al., 2004), the interannual variations of the DC intensity, based on the maximum MLD, has obvious limitations. With a typically low number of in situ profiles and the small area of a DC chimney, the observations may easily miss the deepest DC point, resulting in a bias in the estimate of the DC intensity (see Table 1 and the related discussion). Regular sampling by Argo profiling floats, available in the Greenland Sea since 2002 (Latarius and Quadfase, 2016; Brakstad et al., 2019), has improved the situation. With 5 to 20 profiles per month, Argo alone still gives an insufficient number of observations for obtaining the interannual variability of the maximum MLD, but together with other in situ profiles this forms a sufficient observational basis for correct derivation of the interannual tendencies (Bashmachnikov et al., 2018; Fedorov and Bashmachnikov, 2020). Previous studies also suggest a robust detection of the interannual DC variability with the use of the ARMOR3D data-set, available since 1993 (Bashmachnikov et al., 2019). This restricts the time interval of our analysis.

Another drawback is that assessing the intensity of DC as the maximum MLD, one uses an observation at a single point. However, the main result of the DC, the renewal of the Greenland Sea Deep Water, depends also on the area integral of the chimneys. In this study, the accuracy of the interannual variability of DC (from ARMOR3D data-set) is further confirmed by a second metric, which is the area where the vertical mixing exceeds a certain depth level. We use 800 m as the threshold depth level (S^*_{800}) because this is the upper boundary of the Greenland Sea Deep Water (Rudels et al., 2002; Bashmachnikov et al., 2018). This metric is less dependent on the degradation of the gridded data-set accuracy with depth (see Section 2.1), but it does require using gridded data. A nonlinear relationship between S^*_{800} and *MMLD** is presented in Supplement 7.2. Next in this study we also use S_{800} and the *MMLD* notations for the normalised values. Normalization is done by subtracting the mean and dividing by the standard deviation.

In addition to the direct estimates, several proxy indices of the intensity of DC have been suggested. These indices quantify changes in the thermohaline or hydrochemical properties of sea water (temperature, salinity, oxygen, CFC, etc.), variability of which are supposed to be governed by variations in the intensity of DC (Meincke et al., 1992; Johannessen et al., 1991; Schlosser et al., 1991; Rhein 1996; Bonisch et al., 1997; Alekseev et al., 2001; Azetsu-Scott et al., 2005; Yashayaev, 2007; Rhein et al., 2011; Gladyshev et al., 2016; Bashmachnikov et al., 2019). As the renewed deep water masses spread their properties over the deep areas of the DC basins within a few months, observing such changes in the deep water properties requires substantially fewer observations than one would need for a robust detection of the *MMLD* variations via direct estimates. In the Greenland Sea, the variability of the *MMLD* shows high a correlation with the depth-integrated (100-1500 m) water density averaged over the deep part of the Greenland Basin (Bashmachnikov et al., 2019).

3.3 Oceanic advective fluxes

Following the divergence theorem, we estimate divergence of oceanic fluxes of heat (Q_{adv}), freshwater (FW_{adv}) and density (DF_{adv}), integrated over the study region (Fig. 1), as a surface integral of the fluxes across its lateral boundaries:

$$Q_{adv} = \oiint_{\tilde{S}} \vec{V} \cdot \vec{n}\, C_p \rho_{ref} \left(T - T_{ref}\right) d\tilde{S}, \qquad (1)$$

$$FW_{adv} = \oiint_{\tilde{S}} \vec{V} \cdot \vec{n} \left(\frac{S_{ref} - S}{S_{ref}}\right) d\tilde{S}, \qquad (2)$$

$$DF_{adv} = DF_{T.adv} + DF_{S.adv} = \rho_{ref}\left(-\frac{\alpha}{C_p \rho_{ref}} Q_{adv} - \beta\, S_{ref}\, FW_{adv}\right)$$

$$= \rho_{ref} \oiint_{\tilde{S}} \vec{V} \cdot \vec{n} \left(-\alpha\left(T - T_{ref}\right) + \beta\left(S - S_{ref}\right)\right) d\tilde{S}. \qquad (3)$$

Here the fluxes are integrated over the surface $\tilde{S}$ bounding the study region (positive norm vector $\vec{n}$ is into the study region), *V* is the current velocity, *T* and *S* are the seawater temperature and salinity, respectively, C_p= 3900 J kg^{-1}°C^{-1} is the specific heat capacity. The coefficients of the thermal expansion (α= 0.37 10^{-4} °C^{-1}) and of the salt contraction (β=7.74 10^{-4}) are set to the reference temperature T_{ref}=-1°C and the reference salinity S_{ref}=34.9, while $\rho_{ref} = \rho\,(T_{ref}, S_{ref}, 0)$= 1028 kg m^{-3}. The reference temperature and salinity are taken equal to their typical values in the Greenland Sea Deep Water. The T_{ref} and S_{ref} correspond to the climatic characteristics of the Greenland Sea Deep Water (Nagurniy and Popov, 1985; Alekseev et al., 1989; Moretsky and Popov, 1989; Johannessen et al., 1991; Korablev, 2001). The $\frac{\beta}{\alpha}$ ratio is 21, five times higher than in tropical regions, and shows the strong relative effect of salinity variation on water density in the subpolar waters.

The oceanic meridional advective fluxes are computed across the 73.5°N and 77.0°N sections, extending from the Greenland shelf break across the Greenland Sea and encompassing the region of the most frequent DC (Fig. 1, see also Supplement 7.6). The fluxes are integrated over the whole length of a section and from the sea surface to 500 m depth (after reaching this level the convective renewal of the Greenland Sea Intermediate Water begins).

3.4 Air-sea heat and freshwater fluxes

The net surface heat flux includes surface turbulent (sensible and latent) heat fluxes (Q_{atm}, positive to the ocean) and net shortwave (solar) and longwave radiative fluxes (RB). The net shortwave radiation is the difference between the incoming and outgoing (reflected) shortwave radiative fluxes. Similarly, the net longwave radiation is the difference between the incoming and outgoing surface longwave radiative fluxes, comprising the longwave (infrared) surface emissivity and reflected back atmospheric longwave radiation. The net freshwater flux (net precipitation) at the ocean surface is the difference between precipitation and evaporation.

In the following discussion, we will primarily use net surface heat flux and net precipitation for the DC analysis. In the ice-covered regions Q_{atm} depends on the ice concentration. Whenever the ice concentration is below 15%, the ocean is considered ice-free. For larger ice concentrations, Q_{atm} is integrated only over the ice-free fraction of the grid cell. Adding heat fluxes through the sea ice (Lecomte, 2013), using as an input the ice thickness from the PIOMAS dataset and the climatic snow thickness from Shalina and Sandven (2018), shows practically no effect, neither on seasonal nor on the interannual variability of Q_{atm}. The effect of the ice lid on the surface turbulent heat fluxes (dQ_{ilid}) is computed as the difference between the turbulent heat fluxes over the ocean with no sea ice and over the ocean with the observed ice cover (Q_{atm}). In the regions, where the sea ice is artificially removed, calculation of the sensible heat flux uses the water freezing temperature of -1.8ºC.

To determine the role of cyclones in the variation of the DC intensity, ocean heat and freshwater exchange with the atmosphere are also computed only inside cyclones, detected over the study region. The positions and size of the cyclones were obtained from a data-base of cyclone tracks, derived from the 6-hourly ERA-Interim reanalysis fields (Hoskins and Hodges, 2002; Hodges et al., 2011) , which yields higher number of cyclones than when using mean sea level pressure fields (Vessey et al., 2020). In the data-base the cyclones are detected from the relative vorticity fields at 850hPa. The data are spatially filtered to focus on synoptic scale cyclones by spectrally filtering the data in the T5-42 (triangular truncation, total wavenumbers) band, the cyclones are identified as vorticity maxima on a polar stereographic grid and the locations refined using B-splines and steepest ascent maximization (Hodges, 1995). The identified points are then initially linked together over consecutive time steps using a nearest neighbour method and then are refined by minimising a cost function for track smoothness subject to adaptive constraints on the track smoothness and displacement distance in a time step. The tracks are further filtered to retain only those that travel more than 1000 km and last for more than 2 days. This methodology is described in detail in Hodges (1995, 1999). The cyclone size was estimated from the ERA-Interim mean sea level pressure fields as the last closed air pressure contour.

The density flux through the sea-surface (DF_{oa}) is calculated as a sum of the corresponding net thermal (DF_{atm} and DF_{RB}) and freshwater (DF_{PE} and DF_{ice}) fluxes:

$$\begin{aligned} DF_{oa} = {} & (DF_{atm} + DF_{RB}) + (DF_{PE} + DF_{ice}) \\ & = \rho_{ref}\left(-\frac{\alpha}{C_p\rho_{ref}}(Q_{atm} + RB) - \beta\, S_{ref}(FW_{PE} + FW_{ice})\right), \qquad (4) \end{aligned}$$

where FW_{PE} is the precipitation minus evaporation and FW_{ice} is the freshwater flux from the sea ice formation/melting.

For the purpose of the following analysis, we also distinguish between the density fluxes solely determined by the heat fluxes (DF_T) and solely by the freshwater fluxes (DF_S) as

$$DF_T = DF_{T.adv} + DF_{atm} + DF_{RB} \,, \tag{5}$$

$$DF_S = DF_{S.adv} + DF_{ice} + DF_{PE} \,. \tag{6}$$

4. Results

4.1 Seasonal variability of the DC intensity

In the Greenland Sea, the deepening of the upper mixed layer typically begins in October and continues until April. During October-December the MLD is still shallow, though it deepens and re-stratifies intermittently. Consistent MLD deepening starts in January (Fig. 2a). The month, when the $MMLD$ is reached, varies from year to year. For about 50% of the years (since 1993) the $MMLD$ is observed in April (see also Marshall and Schott, 1999; Kovalevsky, 2002; Fedorov et al., 2018; Bashmachnikov et al., 2018). In late spring, the buoyancy fluxes restore the upper ocean stratification preventing the formation of the DC chimneys (Marshall and Schott, 1999; Kovalevsky, 2002; Kawasaki and Hasumi, 2014; Kovalevsky and Bashmachnikov, 2019). However, observations show that even several months after a DC chimney loses its connection with the sea-surface, water stability in the deep parts of the water column in the Greenland Sea stay low (Wadhams et al., 2004) or may continue to decrease (Kovalevsky, 2002). The percent of the area in the Greenland Sea with DC over 800 m (as well as with DC over 1000 m) shows the same mean seasonal variability (Fig. 2a).

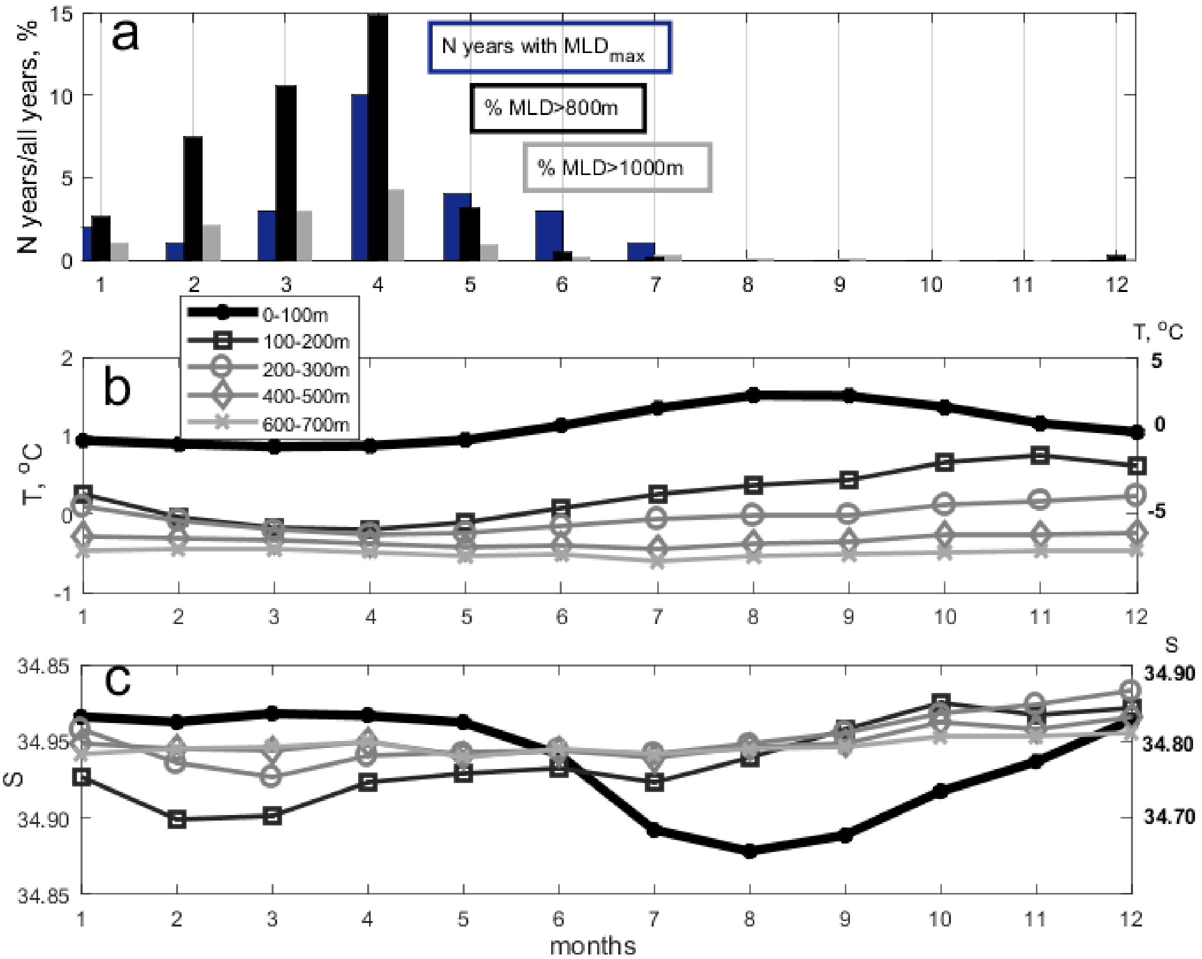

Fig. 2. Seasonal variability of water characteristics in the Greenland Sea: (a) number of years (1993-2016) with DC reaching its annual maximum (blue), from September of the previous year

to August of the current year, and percent of the area in the Greenland Sea with DC over 800 m (black) and with DC over 1000 m (grey); (b) water T, (c) water S. Note that in panels (b) and (c) the amplitude of T and S variations in the upper 100-m is divided by 5 (right scale), in order to variability in the deeper layers becomes visible (left scale).

In the region where DC is frequently observed (the blue trapezoid in Fig. 1), the temperature reaches its minimum in March-April in the 0-300 m layer (Fig. 2b). During the same period the temperature at 400-700 m reaches its annual maximum, i.e. the upper ocean becomes more homogenous. The complexity of the processes governing the variability of the upper ocean density is particularly evident from variations of the upper ocean salinity, which is decoupled from the salinity variation in the top 100-m layer (Fig. 2c). The maximum freshening below 100 m corresponds to the time of the intensive winter vertical mixing, while the following salinification, accompanied by a temperature increase, is a result of RAW advection into the region (Rudels et al., 2002; Jeansson et al., 2008; Langehaug and Falck, 2012).

In the study region, the seasonal variability of the main heat fluxes to the upper ocean are of the same order of magnitude (Fig.3a). The same is true for the main freshwater fluxes (Fig. 3b). During late summer and autumn, the oceanic heat convergence in the upper 500-m layer (Q_{adv}) is positive, and at its seasonal maximum (July – November) and often exceeds RB or Q_{atm} (Fig. 3a). It is during this period when the most intensive warming of the upper ocean below the MLD is observed (Fig. 2b). During the same period, the FW_{adv} stays at its most negative values and far exceeds FW_{PE} and FW_{ice} (Fig. 3b). The advective convergence of more saline water, relative to the salinity of the Greenland Sea Deep Water (S_{ref}, see Section 3.3), leads to an intensive salinification of the upper ocean below the shallow summer MLD (Fig. 2c).

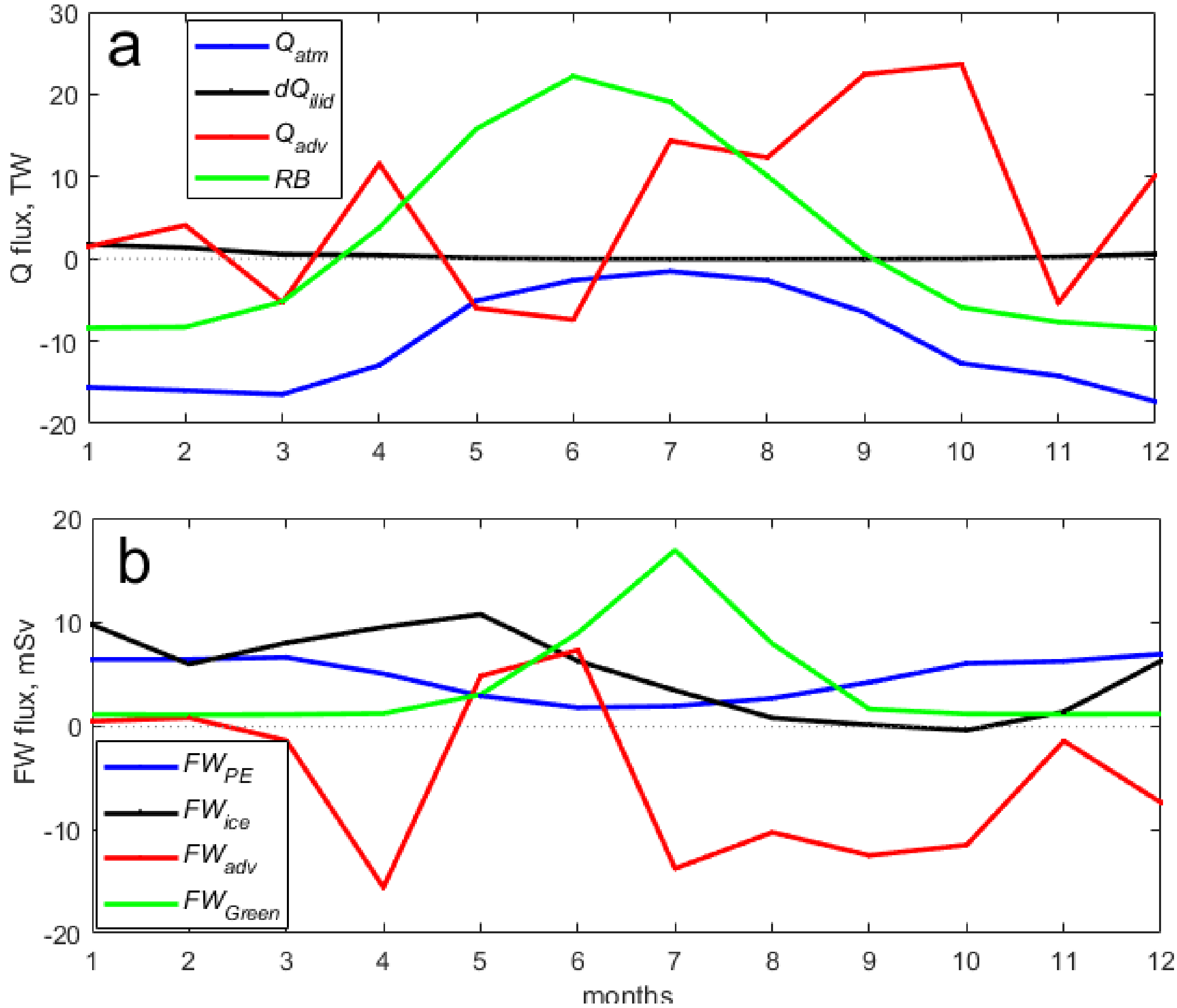

Fig. 3. Seasonal heat (TW) (a) and freshwater (mSv) (b) fluxes in the central Greenland Sea. In (a): Q_{adv} is the heat flux convergence due to ocean advection; $Q_{atm}$is the heat flux from atmosphere to the ocean; dQ_{ilid} is the difference between the heat fluxes from the atmosphere to the ocean when the ice-lid is artificially removed relative to those for the observed ice concentrations; RB is net radiative flux ; In (b): FW_{adv} is the ocean freshwater advection, FW_{PE} is the precipitation minus evaporation; FW_{ice} is the freshwater flux from ice melt; FW_{Green} is the freshwater flux from the Greenland ice sheet in the Greenland Sea.

With the z-axis directed downwards, the vertical gradient of FW_{adv} in the upper 500-m layer (dFW_{adv}, not shown) is always negative (salinity increases downwards), while the vertical gradient of Q_{adv} in the upper 500-m layer (dQ_{adv}) is always positive (temperature increases downwards). This indicates a downward intensification of advection into the study region of RAW that is warmer and more saline than the ambient water .

In winter, the ocean heat loss to the atmosphere (Q_{atm}<0) is attributed to strong negative heat fluxes from the sea surface that far exceed the advective heat fluxes (Q_{adv}). Similarly, the sum of the net precipitation and the sea ice melt exceeds salt advection into the region with the RAW. Over the study region, the seasonal variability of Q_{atm} due to the sea ice cover (dQ_{ilid}) is insignificant (Fig. 3a). For the climatological mean over the study period, dQ_{ilid} is important only along the westernmost part of the region (Supplement 7.3). Greenland freshwater discharge into the Greenland Sea (FW_{Green}) reveals a pronounced summer peak, but in autumn or winter it does not affect the freshwater balance (Fig. 3b).

To summarize, the air-sea fluxes govern the upper ocean winter heat and freshwater balance, while advective fluxes control the upper ocean density variations before the beginning of the DC season. Both processes may be important for the interannual variability of the DC intensity (Fig. 1b).

Furthermore, based on Figures 2 and 3, we define the DC year (from May of the previous year to April of the current year), which is split into the preconditioning season (from May to December of the previous year, further referred as pre-DC season) and the DC season (January to April of the current year).

4.2 Interannual variability of the DC intensity

In this section we discuss the interannual variability of DC intensity in the Greenland Sea deduced from two algorithms: $MMLD$ (Bashmachnikov et al., 2019) and S_{800} (Fedorov and Bashmachnikov, 2020, see also Section 3.1). The Pearson correlation coefficient between $MMLD$ and S_{800} is 0.70 and the Spearman correlation is 0.85; the latter is higher due to the non-linear dependence between the parameters (Supplement 1, Fig. S1). The $MMLD$ metric is more sensitive to variations of the intensity of DC for the winter with weak convection, whereas the S_{800} is more sensitive in the winter with intense DC (Figs. 4a, S1).

The $MMLD$ increases from about 1000 m in the late 1990s to about 2000 m at the end of the 2000s. Since then, a stabilisation and some decrease of the $MMLD$ has been observed (Fig. 4a). This is consistent with the variations of S_{800}. Our results differ from the $MMLD$ variability derived exclusively form the vertical Argo profiles (Table 1, Latarius and Quadfase, 2016), but this is due to an insufficient number of Argo profiles in the study region (see Fedorov and Bashmachnikov, 2020). The low DC in the early 1990s (Fig. 4a) agrees well with the low DC intensity in the 1980s-1990s, derived using various proxy indices (Schlosser et al., 1991; Meincke et al., 1992; Alekseev et al., 2001). The indices also suggest the intensification of the DC during the late 2000s - early 2010s (Bashmachnikov et al., 2019). Therefore, several independent metrics suggest robustness of the detected long-term tendencies in the DC intensity (Figs. 1b and 4).

Next we analyse the relation between the intensity of DC and the upper ocean density. We consider three factors impacting the ocean density (ρ) at a given location: local changes of the upper ocean temperature ($\rho_T = \rho_{ref}\ \alpha T(t)$), local changes of the upper ocean salinity ($\rho_S = \rho_{ref}\ \beta S(t)$), and changes caused by the upwards Ekman suction driven by the cyclonic circulation in the Greenland Sea. A relationship between a doming of isopycnals in the central Greenland Sea and cyclonic vorticity of the Greenland Gyre driven by the cyclonic winds has been demonstrated in previous studies (e.g., Malmberg and Jonsson, 1997; Rossby et al., 2009; Dukhovskoy et al., 2017). We expect the $MMLD$ (and S_{800}) to increase with an increase of ρ_S, of ρ_T and of the mean relative vorticity in the study region (*ω*).

The interannual variability of the upper ocean density is further split into the autumn density (mean over September-December), i.e. accumulated during the pre-DC season, and that at the end of the cold season (April), mostly accounting for the density evolution during the DC season. Besides looking into the interannual variability (Fig. 4a-b), we also analyze the 3-year means (including the current and the two preceding years, Fig. 4c-d). This smoothing reduces the possible errors in the annual $MMLD$ (S_{800}) values, as well as taking into account some preconditioning of the DC intensity during preceding years (Wadhams et al., 2004).

The correlation coefficients of ω with the $MMLD$ and with S_{800} does not exceed 0.10-0.25 and are not significant at 0.05 significance level, for interannual, as well as for the 3-year smoothed results.

The correlation coefficient between the $MMLD$ and ρ for April reaches 0.7-0.8 for the unsmoothed (Fig. 4b) and 0.9 for the 3-year smoothed values (Fig. 4d). The correlation coefficients between S_{800} and ρ in the upper 500-m layer in April reaches 0.6 for the unsmoothed and 0.8 for the 3-year smoothed values. The correlation coefficient between the $MMLD$ (S_{800}) and the mean ρ for the pre-DC season (Fig. 4c) are not significant (from 0.2 to 0.3 for the unsmoothed and from 0.4 to 0.5 for the 3-year smoothed values).

From Figure 4(b-d) we see that, the intensification of DC from the 1990s to the late 2010s coincides with an increase in the winter ρ_S (and ρ), while the tendency of ρ_T contradicts the observed intensification of the DC (note the reverse y-scale in the figure). The Pearson and Spearman correlation coefficients between the $MMLD$ and ρ_S are equally high for the DC season of the current year, as well as for the end of the pre-DC season (0.6 to 0.7 for the annual values and 0.8 for the 3-year means). Correlations with S_{800} are slightly lower, yet significant. The correlations of the $MMLD$ (S_{800}) with ρ_T have the opposite sign at the end of the pre-DC season (-0.3 to -0.8) and are not significant (-0.1 to 0.1) in winter. Also the linear trends of the regional mean winter temperature increase during the study period from 0.5 to 1^{o}C and the salinity – from 34.85 to 34.94. The resulting regional mean ρ_T decreases by 0.02 kg m^{-1} and ρ_S increases by 0.07 kg m^{-1}. Therefore, these are the salinity variations that determine the change in the upper ocean density fields during winter.

To investigate sources of the higher frequency DC variability, we remove the quadratic trends and consider only the non-smoothed interannual variations. For the pre-DC season, the correlation coefficients of the $MMLD$ (S_{800}) with ρ_S , ρ_T and ρ are then not significant (0.1-0.2). For the DC season, the correlation coefficients of the $MMLD$ (S_{800}) with ρ_S (and with ρ) remain significant (0.4-0.5). This means that the upper ocean salinity remains an important factor for the interannual variability of the DC intensity at high frequency.

To summarize, we conclude that the interannual variability in the upper ocean salinity (before and during the DC season) has shaped the interannual, and, in particular, the inter-decadal, variations of the DC intensity in the Greenland Sea since 1993. However, at the end of the study period, some decrease of the DC intensity from 2013 to 2015 cannot be explained by variations of ρ_S , but corresponds to a dominating decrease of the ρ_T (Fig. 4 b-d). Thus, during this latter period, the interannual DC variability can be significantly affected by anomalous heat fluxes.

The unexpected negative correlation of ρ_T with $MMLD$ during the warm season results from a high negative interannual correlation of ρ_T with ρ_S (-0.7). In winter there is some decoupling of the temperature and salinity interannual variations (correlation coefficient decreases to -0.6), which goes along with the drop of the ρ_T correlation with $MMLD$.

The difference between the summer to winter transition in the spatial distribution of the upper ocean temperature and salinity are demonstrated in Figure 5. At the start of the mixing in autumn (October), the tongue of the relatively warm and salty RAW projects into the study region. This penetration becomes deeper during the 2000s (Fig. 5 a-b). However, already at the beginning of the DC season (in January), the upper ocean temperature anomalies disappear or are strongly reduced, while the salinity anomalies continue propagating into the DC region (Fig. 5 c-d). Quantitatively, the long-term effect can be estimated as the linear tendencies of the mean distance between chosen isohalines/isotherms and the western boundary of the study region (the nearest point at the 2000 m isobath along the continental slope). The winter distance for the 34.9 isohaline decreased by about 35% during the study period (from 450 in 1993 to less than 300 km in 2016), whereas that of the 2°C isotherm approaches the shelf break only by about 15% (from 470 in 1993 km to 400 km in 2016), and that of the position of 1°C isotherm practically did not change (at around 350 km from the western boundary).

In summary, the analysis of this section shows that the interannual variability of the $MMLD$ is controlled by the interannual variation of salinity. The mean value of the latter reflects the combined effect of several freshwater fluxes into and out of the study region. Figure 5(b,d) suggests that the interannual variability in salinity might be related to the variability in the intensity of oceanic advection. On the other hand, the excess of the advected heat, accumulated during the warm season, is effectively removed already by the beginning of the DC season: the more heat is accumulated during autumn, the stronger is the ocean heat release during winter. In fact, in the beginning of the DC season, the RB and Q_{atm} stay strongly negative already for three months, while the convergence of heat advection drops nearly to zero (Fig. 3a). The interannual variability of the heat fluxes is analysed in the next Section.

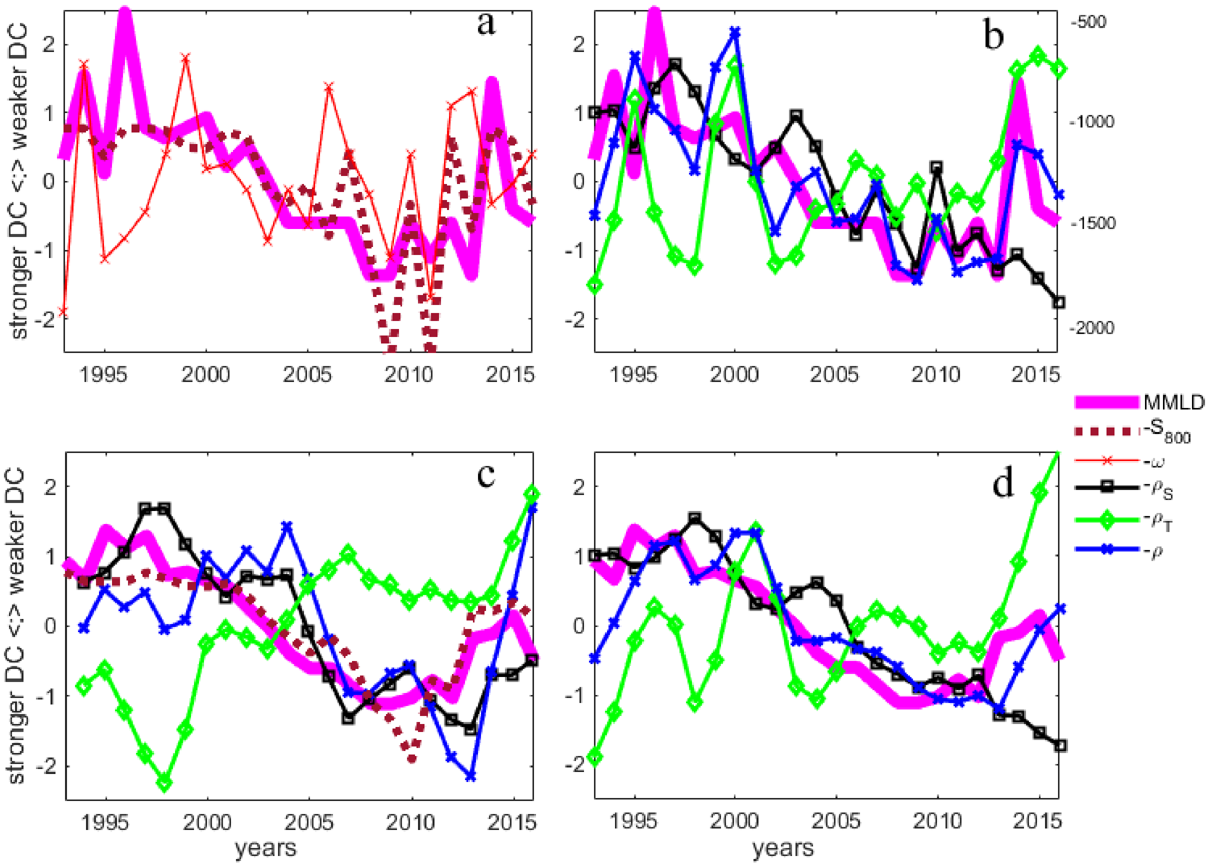

Fig. 4. Interannual variability of the normalised maximum mixed layer depth (MMLD), the areas with MLD over 800 m ($-S_{800}$), the normalised mean relative vorticity in the central Greenland Sea during the DC season (ω), the mean water density of the upper 500 m ($\rho = \rho_0(\beta S - \alpha T)$), the density variability related to changes of ocean salinity ($\rho_S = \rho_0 \beta S$) and to that of ocean temperature ($\rho_T = -\rho_0 \alpha T$). S_{800}, ω and water density are taken with the opposite sign for better visibility. The data are averaged over the study region and normalized by subtracting the respective mean and dividing on the respective standard deviation. Water density in panels (b, d) is given for April, while in panel (c) it is averaged over the pre-DC season. Panels (a, b) present unsmoothed values and panels (c, d) – the 3-year sliding means over the current year and two preceding years.

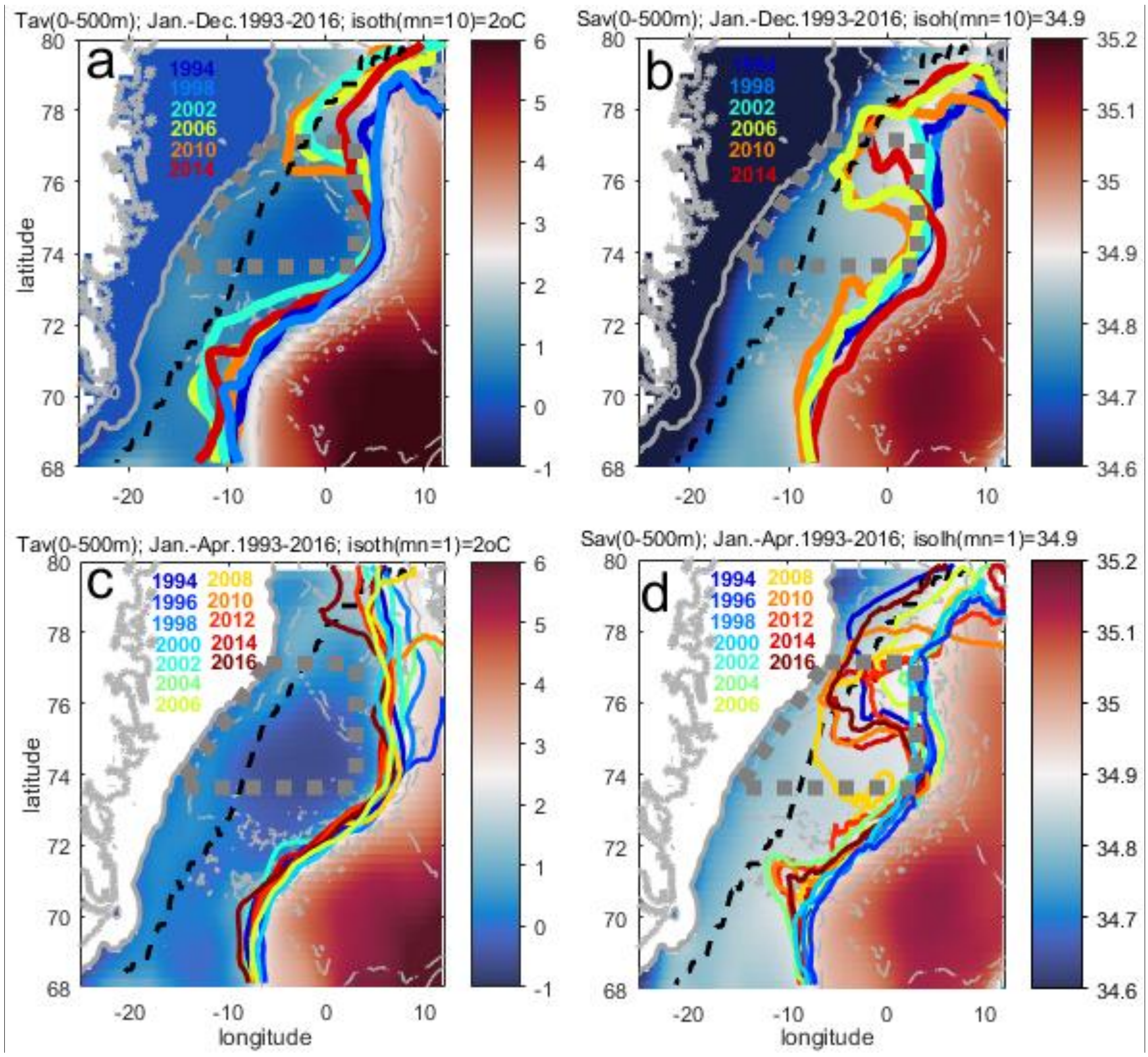

Fig. 5. Time-mean temperature (°C, panels a,c) and salinity (panels b,d) averaged over the upper 500-m layer (ARMOR3D data-set). Upper panels – T was averaged over the whole period of 1993-2016 and lower panels – over the DC season (January to April) only. The 2°C isotherm (panels a, c) and the 34.9 isohaline (panels b, d) are shown for October (upper panels) and January (lower panels) for selected years (see legend in the figures). The isotherm/isohalines are computed from temperature and salinity distributions, averaged over the upper 500-m layer. The thick grey dashed contour indicates the study region. The black dashed line is the mean winter edge of sea ice (PIOMAS data-set). Thin grey lines are the 500-m and 2500-m isobaths.

4.3. Heat fluxes

In this Section we investigate the interannual variability of the dominant heat and freshwater fluxes, which may affect the DC intensity. The heat fluxes considered are (Fig. 6, Table 2): net radiative flux (RB), net air-sea heat exchange (Q_{atm}) and the convergence of the heat fluxes in the upper ocean (Q_{adv}).

$$\frac{dQ}{dt} = RB + Q_{atm} + Q_{adv} + Q_{resid} \qquad (7)$$

For the ice-covered grid cells, deduced from the NSIDC sea ice concentration data, we assume Q_{atm}=0. The term Q_{adv}, represents the bulk warming or cooling of the upper 500-m layer due to convergence of the oceanic heat transport. The horizontal heat flux associated with mesoscale eddies is relatively small in the region, less than 1 TW (from our preliminary analysis not presented here), compared to 3-6 TW coming with the advective transport. The advective flux is referenced to water temperature of the Greenland Sea Intermediate/Deep Water (T_{ref}, Section 3.2). Thus, the negative values favour a possible thermal instability of the water column. The vertical diffusive or convective flux, as well as the horizontal eddy heat flux form the residual term (Q_{resid}).

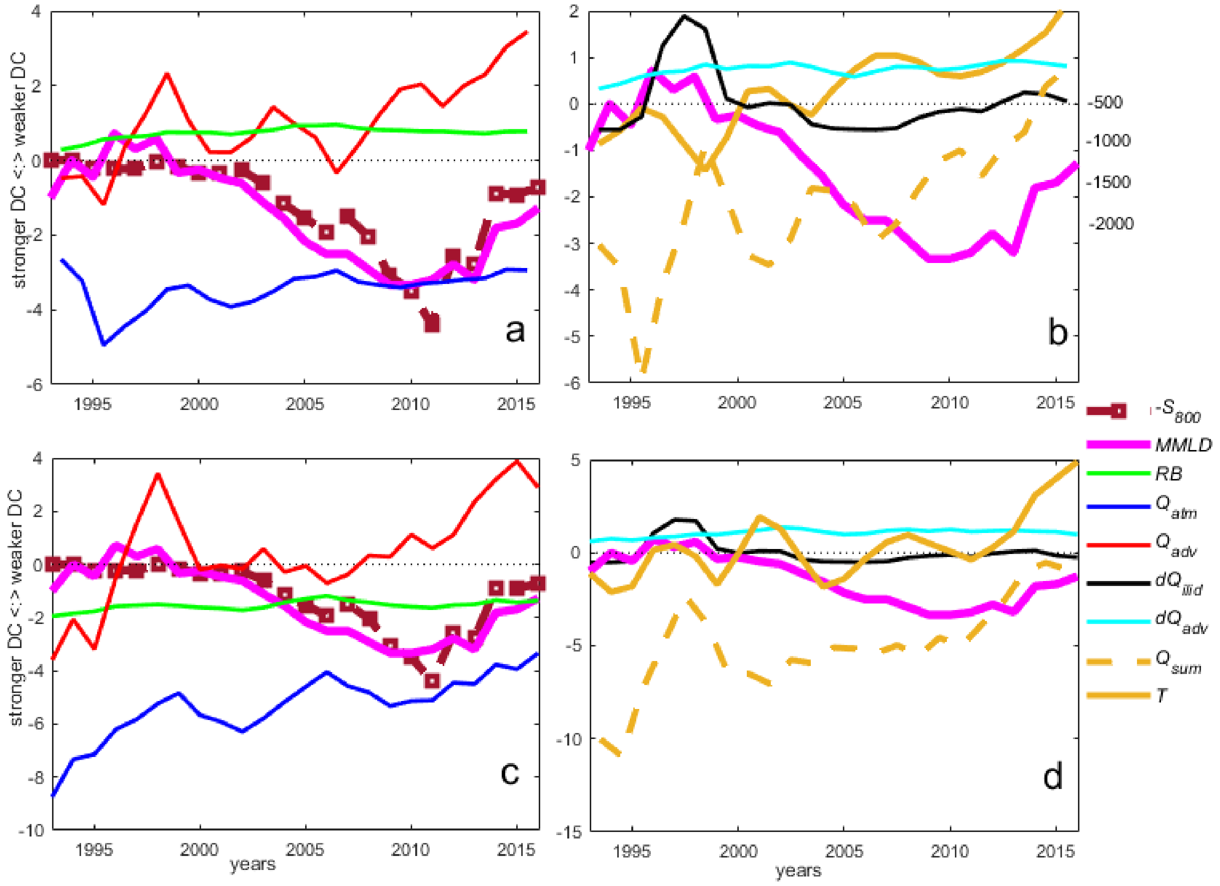

Fig. 6. Interannual variability of mean heat fluxes (TW): (a-b) at the end of the pre-DC season (August-December), (c-d) during the DC season (January to April). Q_{atm} is the sensible plus latent heat fluxes to the ocean, dQ_{ilid} – the effect of ice lid on the ocean-atmosphere heat exchange, RB– the radiation balance, Q_{adv} –the convergence of oceanic heat advection, dQ_{adv} – the mean vertical gradient of Q_{adv} (see text for details). Q_{sum} is the sum of Q_{atm}, RB and Q_{adv} (right panels). All fluxes are normalized by the standard deviation of Q_{atm} for the pre-DC season; positive values favour vertical stability in the upper ocean. T is the mean temperature in the upper 500-m layer (relative units, right panels). Positive fluxes lead to stabilization of the upper part of the water column, decreasing the DC intensity. The DC intensity is represented with the $MMLD$ and S_{800} (taken with the opposite signs, relative units). The right scale in panel (b) presents the $MMLD$ in meters.

Table 2. Heat fluxes (TW), mean values and standard deviations (std). Positive values of the variables lead to stabilization of the water column in the upper ocean. Note that, as in Fig. 6, higher values of $MMLD$ or S_{800} signify a weaker DC intensity. Thus, positive correlations in the table means that the heat input into the ocean flux decreases the DC intensity. Grey cells mark the dominating fluxes with high interannual variability or with a significant correlation. The significant correlations were estimated using the effective degrees of freedom computed as $N_{ef}=(1\text{-}r)\cdot N$ (Thomson and Emery, 2014), where r is the correlation coefficient and N is the number of years. CV is the coefficient of variation which is the standard deviation (std) normalised by the mean value. The pre-DC season is from June to December, the DC season is from January to April. Statistics are obtained from the 3-year sliding averages of the seasonal means. See Table 4 in Supplement 7 for the corresponding density fluxes.

fluxes	mean ±std, monthly means	mean ± std pre-DC season means (3year smoothed)	mean ± std DC season means (3 year smoothed)	CV DC season (%)	Correl. with $MMLD$ (S_{800}), pre-DC/DC seasons
RB (to the ocean)	2.3 ±11.2	4.0 ±0.7	-4.6 ±0.5	10%	-0.6/-0.4 (-0.5/-0.2)
Q_{atm} (to the ocean)	-10.3 ±7.6	-10.2 ±1.5	-15.8 ±3.7	22%	-0.5/-0.5 (-0.3/-0.4)
Q_{adv}(0-500 m)	4.1 ±12.9	3.2±3.5	1.5 ±5.6	1040%	-0.4/-0.1 (-0.3/-0.2)
Q_{adv1} (500-1000 m)	2.3 ±4.4	1.9±1.3	0.5 ±2.4	480%	0.2/-0.1 (0,0/0.0)
Q_{adv2} (0-1000 m)	6.4 ±16.8	5.1 ±4.8	2.0 ±8.0	400%	-0.3/-0.1 (0,2/0.0)
$dQ_{adv} = dQ_{adv}/dz$[up-low]	0.8 ±0.7	0.8 ±0.1	1.2 ±0.2	16%	-0.2/0.2 (0.0/0.0)
dQ_{ilid}	0.4 ±1.7	0.4 ±0.5	1.0 ±1.3	130%	0.5/0.5 (0.4/0.3)

For the time-averaged fluxes, the upper ocean heat loss to the atmosphere (Q_{atm}) clearly dominates the upper ocean heat balance (Table 2). The oceanic heat is released to the atmosphere all year round, being particularly strong in winter (Figs. 3a and 6a,c). In the climatic annual mean, Q_{adv} in the upper 500-m layer, the second largest term in the right-hand side of Eq.(7), is twice the heat coming from RB (though RB strongly exceeds Q_{adv} during the DC season). The Q_{adv} and RB in their annual means oppose Q_{atm} and favour a decrease of the DC intensity. Together these two heat fluxes compensate about 60% of Q_{atm}, while if we account for the heat convergence by ocean advection in the upper 1000 m this is up to 90%. As $MMLD$ exceeds 1000 m for 75% of the winters, this deeper layer should rather be considered for estimating the heat balance in the study region. The situation radically changes during the DC season, when both RB and Q_{atm} destabilise the water column and strongly exceed Q_{adv}.

The high importance of Q_{atm} for the seasonal variability of DC in the Greenland Sea, makes many researchers consider Q_{atm} as the main driver for the DC interannual variability (Jones and Marshall, 1993; Bailey et al, 2005; Falina and Sarafanov, 2015; Moore et al., 2015; Yang et al, 2016). However, the standard deviation (and the coefficient of variation) of the interannual variability of Q_{adv} exceeds that of Q_{atm} almost by a factor of two in winter and by a factor of three in summer (Table 2). These ratios further increase, if the oceanic heat flux convergence is integrated down to 1000 m. This suggests that, the interannual variability of Q_{adv} may have a higher importance for the variability of the upper ocean stratification on the interannual time scales than that of Q_{atm}.

Since 1993, both Q_{atm} and Q_{adv} show positive trends, which result in an overall increase of Q_{sum} over the time period from 1993 to present (Fig. 6b,d). This is consistent with the increase of the upper ocean temperature in the study region (Fig. 6b,d). This long-term temperature trend is less pronounced in winter (there is practically no trend, except during 5 years at the end of the study period, Fig. 6d). We assume that, in winter, large Q_{atm} and RB effectively abate interannual variations of Q_{adv} (see Fig. 5c and Supplement 7.4).

In addition to Q_{adv}, accounting for a possible thermal convective instability below the upper 500-m layer, we also estimate the effect of the convergence of oceanic advective heat fluxes on the static stability of the upper 500-m layer (dQ_{adv}). The dQ_{adv} is defined as $\partial Q_{adv}/\partial z$ averaged over the upper 500-m layer. Positive values of dQ_{adv} suggest stronger warming in the upper part of the layer (due to the horizontal heat advection) relative to the lower one. Always positive values of dQ_{adv} signify that the ocean heat advection stabilizes the upper 500-m of the water column all year round (Table 2, Figs. 6b,d). However, the coefficient of variation of dQ_{adv} is low, suggesting a small relative interannual variability of this parameter and a minor role of this effect in the interannual variability of DC.

The correlation of most of the heat fluxes with the $MMLD$ (S_{800}) are predominantly negative. Therefore, an increase of the DC intensity during the study period coincides with more heat absorbed by the upper ocean (Table 2), which is counterintuitive. For an explanation we direct the reader to Supplement 7.4 and discussion below.

The hypothesis of Moore et al (2015) on the possible variability of DC intensity due to the modification of Q_{atm} by the ice cover in the central Greenland Sea, is examined by introducing an additional variable dQ_{ilid}. To single out the effect of the ice-lid, dQ_{ilid} is computed as the difference between the possible latent and sensible heat fluxes over the sea ice covered areas, computed as if the sea ice is absent, and the previously estimated Q_{atm}, which takes into account a real ice cover. The positive values of dQ_{ilid} account for the suppression of the DC by the ice cover. On average, the effect of ice cover (dQ_{ilid}) is small, compared to other terms of the heat balance (Table 2), and it does not explain the long-term tendencies in the DC intensity (Fig. 6b,d). However, episodically dQ_{ilid} might become important. Thus, during the winters of 1996/1997 and 1997/1998 (Fig. 6), the anomalously weak DC corresponds to the anomalously big Oden ice tongue projecting far into the central Greenland Sea (Comiso et al., 2001; Germe et al., 2011). The interannual variability of the Odden ice tongue is linked to the wind direction, mostly intensified during the negative North Atlantic Oscillation (NAO) phase (Germe et al., 2011). The long-term tendencies in dQ_{ilid} may also be shaped by the intensity of the oceanic heat advection with RAW, which becomes weaker at the negative NAO phase (Selyuzhenok et al., 2020), though we did not find a clear indication of this link within the study period.

To conclude, all heat fluxes, except dQ_{ilid}, are weakly or inversely correlated with the $MMLD$ (S_{800}). A long-term increase of the heat input into the study region, which goes in parallel with an increase of the upper ocean temperature, contradicts the observed intensification of the DC during the 2000s (Fig. 6). This counterintuitive "reaction" of the $MMLD$ results from its dependence on the freshwater fluxes (see Section 4.2), while the main freshwater fluxes are inversely correlated with the heat fluxes. For example, the major source of the interannual variability of the upper ocean heat content, Q_{adv}, is inversely correlated with the FW_{adv} (-0.54), i.e. the oceanic heat and salt transport in the region increases/decreases simultaneously (see also Supplement 7.4). The freshwater fluxes are discussed in the next section.

4.4. Freshwater fluxes

Components of the Greenland Sea freshwater budget are net precipitation (FW_{PE}), net sea ice melt (FW_{ice}) and convergence of the freshwater advection in the upper ocean (FW_{adv}):

$$\frac{dFW}{dt} = FW_{PE} + FW_{ice} + FW_{adv} + FW_{resid}. \quad (8)$$

The first three terms on the right-hand side of Eq. (8) are approximately of the same order of magnitude (Fig. 7, Table 3). The convergence of advective freshwater fluxes between 500 and 1000-m is negligibly small compared to FW_{adv} in the upper 500-m layer. The freshwater from the Greenland Ice Sheet (FW_{Green}) is listed in Table 3 for reference. It does not affect the central areas of the study region, as all the meltwater is advected out of the sea by the EGC (Dukhovskoy et al., 2019). Thus, FW_{Green} is not included in the following analysis.

One can easily see (Table 3) that positive FW_{PE} and FW_{ice} are not balanced by the negative FW_{adv}, neither in the annual nor in the seasonal means. Therefore, unlike the residual heat flux, FW_{resid} has the same order of magnitude as each of the terms in right-hand side of Eq. (8) (on average 5 mSv, ranging from 0 to 10 mSv). The FW_{resid} includes the vertical freshwater exchange due to convection or vertical mixing and the deep water outflow below 1000 m, as well as the eddy transport. These fluxes are largely uncertain. In particular, the vertical mixing during the DC episodes effectively redistributes the freshwater over the water column (Dukhovskoy et al., 2019). The freshwater further outflows from the study region at 1000-2000 m as the Greenland Sea Deep Water (see, for example, Jochumsen et al., 2012; Buckley and Marshall, 2016; Kovalevsky and Bashmachnikov, 2020). Available estimates suggest that the total freshwater outflow from the Greenland Sea may exceed 100 mSv (Vage et al., 2013; Chafik and Rossby, 2019). Even though 95% of the outflow belongs to the upper ocean (Vage et al., 2013), the remaining 5 mSv at depth are sufficient to close the balance.

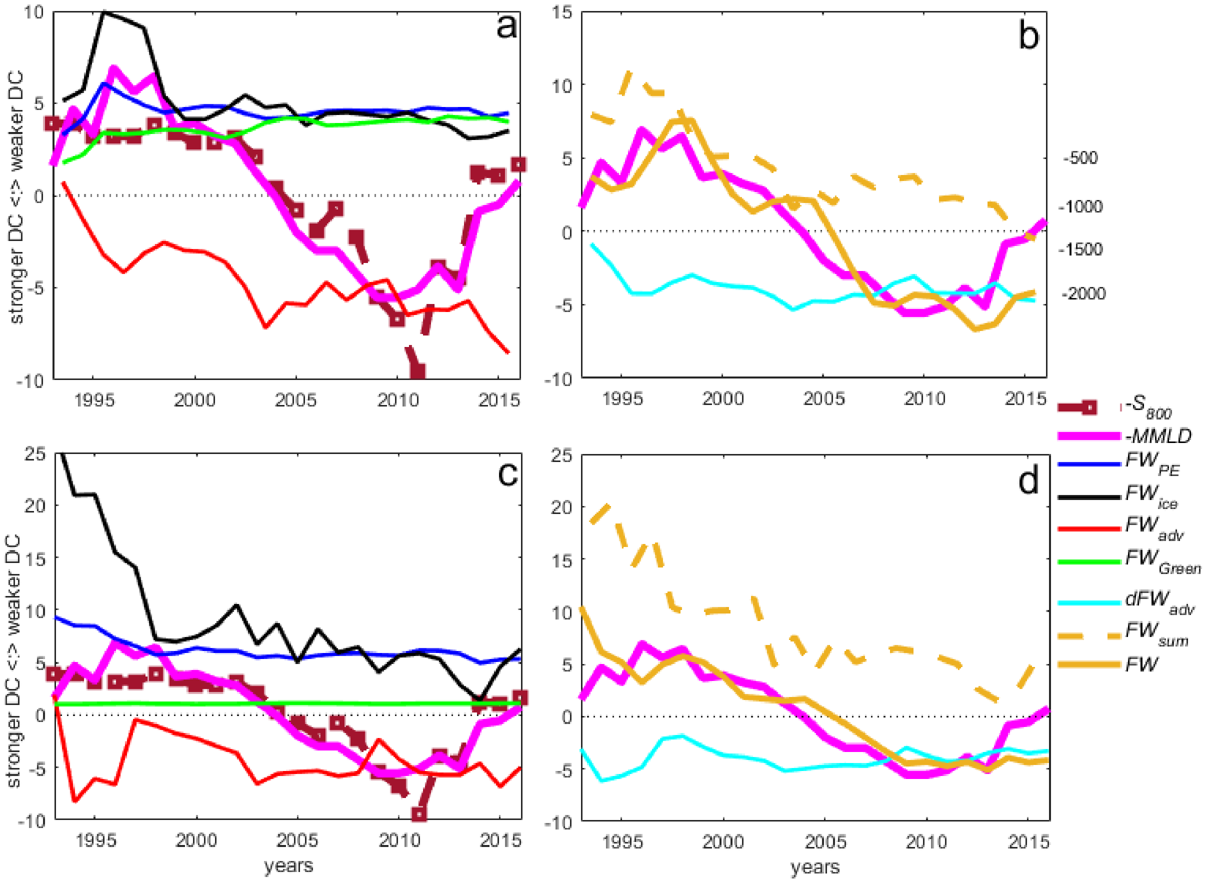

Fig. 7. Interannual variability of mean freshwater fluxes (mSv): (a-b) by the beginning of the DC season (August-December), (c-d) during the DC season (January to April). FW_{PE} is the precipitation minus evaporation, FW_{ice} – the freshwater from ice melt/freezing, FW_{adv}–the convergence of oceanic freshwater advection, FW_{Green} – the freshwater from melt of Greenland ice cap in the Greenland Sea, dFW_{adv} – the mean vertical gradient of FW_{adv} (see text for details). FW_{sum} is the sum of FW_{PE}, FW_{ice} and FW_{adv} (right panels). All fluxes are normalized by the standard deviation of FW_{PE} for the pre-DC season; positive values favour vertical stability in the upper ocean. The regional mean salinity anomaly (FW, relative units, higher values means a fresher water) is presented in the right panels. Positive fluxes lead to stabilization of the upper part of the water column, decreasing the DC intensity. The DC intensity is represented with $MMLD$ and S_{800} (taken with the opposite signs, relative units).

Table 3. Freshwater fluxes (mSv=10^3 m^3 s^{-1}), mean values and standard deviations (std). Positive values lead to stabilization of the water column in the upper ocean. Note that, as in Fig. 7, higher values of $MMLD$ or S_{800} signify a weaker DC intensity. Thus, positive correlations in the table means that the freshwater input into the ocean decreases the DC intensity. Grey cells mark the dominating fluxes with high interannual variability or the significant correlations. The significant correlations were estimated using the effective degrees of freedom (see Table 2). The pre-DC season is from June to December, the DC season is from January to April. Statistics are obtained from the 3-year sliding averages of the seasonal means. When multiplied by the factor of 3, the freshwater fluxes (in mSv) have the same effect on water density as the heat fluxes (in TW) from Table 2. See Table 4 in Supplement 7 for the corresponding density fluxes.

types of fluxes	mean ±std, monthly means	mean ± std pre-DC season means (3year smoothed)	mean ± std DC season means (3 year smoothed)	CV DC season (%)	Correl. with $MMLD$ (S_{800}), pre-DC/DC seasons
FW_{Green}	*3.8 ±4.9*	*3.7 ±0.5*	*1.1 ±0.0*	*5%*	-0.7/-0.4 (-0.6/-0.2)
FW_{PE}	4.7 ±2.3	4.6 ±0.5	6.2 ±1.1	18%	0.3/0.4 (0.1/0.4)
FW_{ice}	5.1 ±8.6	5.1 ±1.9	9.0 ±6.3	70%	**0.7**/0.5 (0.4/0.5)
FW_{adv} (0-500 m)	-5.1 ±9.2	-4.5 ±2.3	-4.4 ±2.4	55%	**0.6**/0.3 (0.5/0.2)
FW_{adv1} (500-1000 m)	0.04 ±1.1	0.1 ± 0.4	0.50 ± 0.50	100%	0.2/0.3 (0.2/0.3)
FW_{adv2} (0-1000 m)	-5.1 ±9.9	-4.4 ±2.5	-3.9±2.7	70%	**0.6**/0.3 (0.5/0.3)
$dFW_{adv} = dFW_{adv}/dz$[up-low]	-1.4 ±1.4	-1.3 ±0.3	-1.3 ±0.4	31%	0.2/0.1 (0.1/0.0)

The interannual variability of the net freshwater flux is dominated by the FW_{adv} and FW_{ice}; the variability of each of these fluxes exceeds two to six times that of FW_{PE} (Table 3).

High positive correlations of FW_{ice} and FW_{adv} with the $MMLD$ (Table 3) suggest an expected decrease of the DC intensity with a higher freshwater input. However, these two freshwater fluxes are not independent. We found a positive correlation of FW_{ice} with the oceanic heat inflow to the region in the upper 100-m (the correlation coefficient is 0.45). A previously derived coupling of an increase of the ice volume and RAW inflows into the Greenland Sea favours a stronger ice melt in the study region during these episodes (Selyuzhenok et al., 2020, see also Fig. 7a,c). Further, a stronger RAW advection also destabilises the upper water column and uplifts deeper warm RAW water to the ocean surface which increases the ice melt (Selyuzhenok et al., 2020; see also Section 4.3 and Supplements 7.5-7.6).

In spite of an increase in the ice melt, the annual mean salinity in the DC region has been increasing since 1993 (Fig. 4c,d, note the reverse vertical axis in the figure). An increase of water salinity in the DC region could be attributed to a stronger advection of RAW (Fig. 5c,d). Negative all the year round, the absolute value of FW_{adv} starts exceeding FW_{ice} (in the annual mean) after the beginning of the 2000s (Fig. 7a,c). The decreasing effect of the ice melt on the DC intensity during the 2000s is also due to a westwards retreat of the marginal ice zone, towards the EGC, with an increase of the sea-surface in the Greenland Sea (Selyuzhenok et al., 2020; see also Fig. 6b). With the EGC, a stronger outflow of the sea ice meltwater from the study region is observed (Fig. S2e). As a result, the joint decrease of FW_{adv} and FW_{ice} during the 2000s (Fig. 7a,c) leads to the positive salinity trend in the study region and a stronger DC intensity (Fig. 4c,d).

To summarize, oceanic advection of salt with the RAW appears to be the most important factor in controlling the long-term interannual variability of DC intensity in the Greenland Sea during the study period (see also Fig. 5). A relatively small effect of heat advection compared to the freshwater (salt) advection in the overall upper ocean density advection into the study region is discussed in Supplement 7.7. A synergy of the extent of the ice cover and of the upper ocean RAW advection may also be responsible for an episodic year-to-year variation in the DC intensity (via variability FW_{ice} and dQ_{ilid}). However, overall FW_{ice} is concentrated in the western part of the DC region and does not affect the areas of the most frequent DC development (Fig. S2e).

4.5 The transient forcing of extratropical cyclones and polar lows

Besides the mean heat release from the ocean to atmosphere, the extreme heat release, which may be linked to cyclonic activity, can be a factor in the interannual variability of DC. In cyclones the vertical heat fluxes from the ocean can grow several times compared to the climatic means and cyclones can trigger fast DC development (Kovalevsky et al., 2020). Over the course of the 24-year study period, 325 long lived cyclones covering at least 20% of the DC area that translated over the region were identified (Hodges 1995, 1999; Hoskins and Hodges 2002). For every cyclone within the study region, the sensible and latent heat fluxes to the atmosphere were estimated using the Coupled Ocean–Atmosphere Response Experiment algorithm (COARE 3.5; Fairall et al., 2003). The resulting mean and integral heat flux in the cyclones inside the DC region (as well as in its sub-region with the maximum DC frequency – Fig. 1a) were recorded.

The extreme vertical heat winter fluxes in the cyclones reached 400-500 W m^{-2}, compared to about 100 W m^{-2} of the winter regional average. However, the mean winter heat fluxes over all cyclones of 115 W m^{-2} was close to the regional mean and only in about half of the recorded cyclones the regional mean values were exceeded. The absence of a statistically significant increase of mean heat fluxes in a cyclone has been noted previously for the North Atlantic (Rudeva and Gulev, 2011).

To explore any relation with the DC intensity, the air-sea heat fluxes in the cyclones were integrated in time from the beginning of November of the previous year until the month of the maximum $MMLD$ event. The sensitivity tests showed that the choice of the starting month for the integration within the pre-DC season (August to December) had almost no impact on the results. Another calculation was performed in the same way, but the heat fluxes were integrated only over those cells, where combined sensible and the latent heat fluxes exceeded the corresponding monthly mean value. Correlation between the interannual variability of integrated heat fluxes and of $MMLD$ did not exceeded 0.3-0.4 (at maximum being of marginal significance). Similar values are obtained when considering only cyclones within the smaller region of the most frequent DC (Fig. 1a). To better assess the influence of cyclones with extreme heat fluxes on DC intensity, we computed monthly mean and monthly maximum heat fluxes in the cyclones for both, values integrated over the areas of the cyclones and the not integrated ones. Next, mean and maximum values over the period of integration were correlated with the interannual variability of $MMLD$. The resulting correlations were also low, with about 0.4 for the case when mean values are used and about 0.3 when using maximum values. Overall, this indicates only a weak dependence of the interannual DC intensity on variations in cyclone-induced ocean-atmosphere heat exchange.

The role of mesoscale atmospheric patterns on the DC intensity, however, requires further investigation. In particular, in some case studies extremely high heat fluxes were observed in the transition zones between cyclones and anticyclones (Lui et al., 1997). In addition, polar lows, which are short-lived intense mesoscale cyclones, are also observed in the DC region (Rasmussen and Turner, 2003). To assess their possible influence on the DC intensity we used a satellite-derived polar low list available for 1995-2009 (Smirnova et al., 2015). The analysis considered polar lows that occurred from November to the month of the maximum $MMLD$ event. Over the 14-year period, a total of 56 polar lows that covered at least 20% of the DC region area were identified. The number of events might be insufficient for deriving a meaningful statistical relationship between the air-sea heat fluxes in the polar lows and the DC intensity. Therefore, the identified polar lows were combined with the data set of extratropical cyclones to deduce the relationship between the air-sea fluxes and the DC intensity. This approach, however, did not result in higher correlation (compared to the array of extratropical cyclones only presented in the previous paragraph). The mean heat fluxes in polar lows of 122 W m^{-2} were close to the regional mean values, although slightly higher than in extratropical cyclones. Only in 30 cases, the mean fluxes exceed the monthly mean values. It should be noted that polar lows are poorly resolved in ERA-Interim leading to substantial negative bias in the maximum wind speeds in the cyclones (e.g., Smirnova and Golubkin, 2017), which apparently results in underestimated air-sea heat fluxes. Condron and Renfrew (2013) found substantial influence of polar mesocyclones on DC in the Nordic seas using model experiments forced with atmospheric reanalysis wind fields corrected by implementing a parameterization of Rankine vortices to better represent polar mesocyclones. However, their number of artificially parameterized polar mesocyclones in the North Atlantic (about 2000 per year) far exceeds the annual mean polar low numbers found in satellite-based studies (e.g., less than 50 in Golubkin et al. (2021) for a slightly larger area). Overall, given the small number of polar lows over the DC region (about 4 per season, as has been derived from the available data-sets), we assume their negligible impact on the interannual variability of the DC intensity.

Cyclones may additionally affect the DC intensity via FW_{PE} or ice advection by wind. We found that the interannual variations of FW_{PE} in the cyclones were small, compared to other parameters of the freshwater balance (Table 3) and did not to have a significant effect on the

DC intensity. There are also practically no correlations with the DC intensity (below 0.2) of the number of cyclones, or of the total time when the cyclones were observed over the DC region. Therefore, in spite of several understudied effects, we assume the overall small effect of cyclones on the interannual variability the intensity of DC in the Greenland Sea.

5. Summary and Discussion

Various mechanisms have been suggested to govern the interannual variability of the intensity of DC in the Greenland Sea such as the cyclonic circulation in the central Greenland Sea (Clarke and Gascard, 1983), upper ocean cooling associated with intense air-sea heat fluxes (Marshall and Schott, 1999; Moore et al., 2015; Yang et al, 2016), presence of sea ice reducing the air-sea heat exchange (Mysak et al., 1990; Moore et al., 2015; Vage et al., 2018), the oceanic buoyancy advection into the central Greenland Sea (Johannessen et al. 1991; Alekseev et al., 2001; Zang et al., 2004; Dickson et al., 2008; Glessmer et al., 2014; Lauvset et al., 2018; Brakstad et al., 2019), the sea ice and the Greenland Ice Sheet melt (Dukhovskoy et al., 2016). Two main problems in understanding the major mechanisms driving the interannual variability of DC in the Greenland Sea can be highlighted.

The first problem is the choice of a robust metric that realistically quantifies the interannual variability of the DC. A low number of available in situ vertical profiles may result in wrong interannual tendencies in the intensity of DC (Fedorov and Bashmachnikov, 2020). In Fedorov and Bashmachnikov (2020) it has been demonstrated that the number of in situ vertical profiles in the Greenland Sea is sufficient for the estimation of interannual variability of the $MMLD$ with at least 25% accuracy (250 m for $MMLD$= 1000 m) for 85% of the years since 1993. In this study we use the ARMOR dataset, which benefits from combining individual in situ profiles with satellite data (see Section 2.1). This increases the robustness of the final gridded fields. Compared to GLORYS and SODA, ARMOR shows a shallower maximum convection depth (Table 1). This is presumably due to insufficient in situ data for deep layers replaced by climatological hydrographic fields below 1500 m in the ARMOR dataset. Nevertheless, the tendency in interannual variability of the $MMLD$ in the Greenland Sea since 1993, derived from the $MMLD$ of ARMOR, is reproduced in the ocean reanalysis products (SODA, GLORYS), as well as various complementary indices: the integral density (Bashmachnikov et al., 2019) and the deep water temperature (Alekseev et al., 2001). In this study, the robustness of these tendencies is additionally supported by S_{800} metrics, which are not affected by possible biases in the deep ocean hydrography in ARMOR (the correlation between the S_{800} and the $MMLD$ is 0.7 on monthly, as well as on interannual time scales). Various data sets and metrics of the DC intensity show that the tendency for DC intensification from the 1990s to the end of the 2000s and its further stabilization during the 2010s, are robust and can be used for analysis of the related mechanisms.

The long-term tendencies in the $MMLD$ and S_{800} are governed by the variability of the upper ocean (0-500 m) density (including that before the DC season) in the central Greenland Sea (Fig. 4). In the subsurface layers, upward-doming ispoycnal surfaces driven by the cyclonic circulation in the Greenland Sea are considered as an important pre-convection condition that determines the intensity of the deep convection in the following winter. However, this study did not find any notable links between the interannual variability of the ispoycnal depths in the central Greenland Sea and the intensity of the DC during the study period (Section 4.2).

Another problem is the strong association between the interannual variability of various heat and freshwater fluxes, each of which may govern the interannual variability of the DC intensity. The interannual variability of the upper ocean temperature or salinity reflects possible imbalance of the heat or freshwater fluxes. We found that salinity plays the leading role in the interannual variability of the upper ocean density and the DC intensity (Section 4.2), whereas the interannual variability of the upper ocean temperature is by far less important.

The leading role of salinity, advected into the Greenland Sea with the RAW, in modifying the density of the upper Greenland Sea has been noted in several studies (Johannessen et al., 1991; Alekseev et al., 2001; Marnela et al., 2013; Glessmer et al., 2014; Deshayes et al., 2014; Boning et al., 2016; Lauvset et al., 2018). There are two reasons for this. First, we found an effective damping of the variability of the oceanic heat transport, the flux with the largest amplitude of interannual variations among the heat fluxes in the study region. The magnitude of the oceanic heat flux variability is strongly abated before it reaches the convective sites in the Greenland Sea, reducing its impact on the DC. Second, the ratio $\frac{\beta_s}{\alpha_t}$ in the subpolar regions is five times that in the tropics. This demonstrates a relatively large effect of water salinity on the variability of water density in the subpolar areas (see also Ferreira et al., 2018). Therefore, among the number of interlinked fluxes, the mechanisms of the DC variability should be primarily governed by the freshwater fluxes (see Table 4). The buoyancy fluxes are considered not only within the DC season, but also accumulated during the preceding warm period.

Among the main freshwater fluxes (FW_{PE}, FW_{adv}, FW_{ice} and FW_{Green}), interannual variations of the oceanic freshwater advection (FW_{adv}) and of the ice melt (FW_{ice}), are found to be the most important for the interannual variability of the DC intensity in the Greenland Sea (Section 4.4). In the upper 500-m layer, advection of salt increases towards the sea-surface, which leads to a decrease of stability of the water column. The negative FW_{adv}, on average, leads to a salinification of the upper ocean, while the positive FW_{ice} – to its freshening (Figs. 5, 7 and S2e). The tendency for salinification of the upper ocean in the central Greenland Sea during the 2000s (Fig. 4b,d) corresponds to a tendency for FW_{adv} to become more negative and to a decrease of FW_{ice} in the study region over the 24 year period of the study (Fig. 7a,c). This study develops further the results by Johannessen et al. (1991), Alekseev et al. (2001), Dickson et al. (2008), Chatterjee et al. (2018), where the role of RAW in forming the salinity of the upper Greenland Sea was highlighted. Here we showed the role of RAW in shaping the long-term interannual variability of DC through the analysis of the variability of the major heat and freshwater fluxes in the region. The intensity of the RAW inflow into the region is regulated by water transport, as well as by the thermohaline water properties in the WSC (Chatterjee et al., 2018), while its effect on the variability of FW_{adv} (and Q_{adv}) in the study region through the RAW recirculation, as well as the degree of RAW modification along the recirculation branches with the Polar Water still remains to be understood.

We also found that during the years of intensive DC, ice meltwater from the Greenland Ice Sheet (FW_{Green}) also increases (Table 2). The correlation coefficients between the variables are high (0.7), although the Greenland ice melt water only weakly affects its central areas (Dukhovskoy et al., 2019). We suggest that this link can be induced by a more intensive warm and salty RAW advection in the shelf of Greenland. Entering the Greenland shelf below the Polar water, the stronger heat flux accelerates the melt of Greenland glaciers (Johannessen et al., 2011, 2013).

The yearly main heat fluxes (RB, Q_{atm}, Q_{adv}), forming the variability in water temperature in the DC region, on average are in an approximate balance. Contrary to what has been suggested in a number of other studies, the interannual variability of the oceanic heat release to the atmosphere appears to be far less important for the interannual variability of the heat balance than Q_{adv}, even during the DC season. Thus, our results show that the interannual variation of Q_{atm} are significantly smaller than those of Q_{adv}, in spite of Q_{adv} (even in its autumn extreme) that forms only about 30% of Q_{atm}.

The two fluxes in the study region are linked as the correlations between winter $|Q_{atm}|$ and $|Q_{adv}|$ varies from -0.6 (detrended) to -0.8 (original). The heat, advected by the ocean, is effectively released to the atmosphere by way of the RAW to the DC region. From one side, this decreases the effect of Q_{adv} on the upper ocean density in the study region. In fact, the winter variability of upper 500-m water density, advected across the northern boundary into the study region, is a function of water salinity (the correlation coefficient is 0.77) and is very weakly linked to water temperature (the correlation coefficient is -0.12) (Fig. S5 in Supplement 7.7). From the other side, Q_{adv} affects the interannual variability of Q_{atm} over the study region. There is a clear tendency for the air temperature and humidity to increase in time. The increase is particularly strong over the pathway of the RAW, in particular north and east of the study region (see Fig. S3a,c in Supplement 7.4). The warmer more humid air is further spread over the study region by the northerly winds (Fig. S3b), which decreases the heat release by the ocean (Fig. S3d). As a result of such a link, the increasing Q_{adv} leads to a decrease of Q_{atm} in the areas of the most frequent DC development since 1993. The tendencies in both fluxes result in an increase of the upper ocean temperature in the areas of the DC development (Fig. 6). However, temperature does not play the leading role in the long-term variability of the DC intensity during the study period (Fig. 4).

The ice cover may have a double effect on the DC intensity – through baring the ocean-atmospheric exchange (dQ_{ilid}) and through contributing to the freshwater balance of the melting/freezing ice (FW_{ice}). The FW_{ice} is not only one of the largest terms in the freshwater balance of the central Greenland Sea, it also strongly correlates with the DC intensity. However, the direct effect of FW_{ice} is mostly limited to the western part of the region (Fig. S2d). In the eastern area of the most frequent development of the DC, the mean effect of FW_{ice} decreases by an order of magnitude. This freshwater is concentrated at the very sea-surface and the way it spreads over the central Greenland Sea is not well understood.

On the contrary, during the study period, the effect of dQ_{ilid}, on average, is small (Table 2). However, during some winters, dQ_{ilid} may decrease the ocean heat flux to the atmosphere by as much as 30-50% (Table 2, Fig. 6). Since 1993, during the 24 years of the study period, this happened for only two winters (of 1996/1997 and of 1997/1998), but it might happen more frequently before 1993 with the development more often of the Oden ice tongue (Comiso et al., 2001; Germe et al., 2011). On the other hand, both dQ_{ilid} and FW_{ice} are partly shaped by Q_{adv} and Q_{atm} and cannot be considered fully independent variables.

The annual mean Q_{atm}, Q_{adv} are strongly correlated with RB (0.7-0.8). Besides a stronger heat release by the ocean surface (Q_{atm} and RB) over the core of the RAW along the EGC (a larger Q_{adv}), all three parameters may depend on a third factor. The oceanic advection in the Nordic Seas intensifies with an intensification of the cyclonic atmospheric circulation around the Icelandic minimum during the positive NAO phase (Yashayaev and Seidov, 2015; Chatterjee et al., 2018; Selyuzhenok et al., 2020). Thus, the high correlation of ocean-atmosphere heat exchange with the radiative heat fluxes (clouds) and with the intensity of ocean heat/freshwater advection may all be a result of the intensification of the regional cyclonic wind pattern.

The observed increase in the RAW advection, is consistent with the AMOC intensification in the North Atlantic during the 1990s, followed by a certain AMOC slowdown in the 2010s (Rahmstorf et al., 2015 Chen and Tung, 2018). However, we lack observations to verify this link as the period since 2004, covered by RAPID observations, only shows a short period of relatively stable AMOC intensity (Volkov et al., 2020). The possible link between the convection and the RAW transport intensities suggests a possible positive feedback between the AMOC on variability of the DC intensity in the Greenland Sea, previously described for the Subpolar Gyre, i.e. Labrador and Irminger seas (Levermann and Born, 2007; Bower and von Appen, 2008; Born et al., 2013). The intensified AMOC leads to a stronger RAW inflow in the Nordic Seas, which increases the water salinity in the central Greenland Sea. The further increase of the convection intensity presumably increases the dense water outflow through the Denmark and the Faroe-Shetland straits. The possible existence of this feedback, though acting at much larger time scales, which includes convection in the Greenland Sea, has been derived in some model studies (see, for example, Renold et al., 2010). At the time scales discussed in this study, this hypothetical feedback can be abated and masked by numerous intermediate and external effects. First, observed increase in salinity in the central Greenland Sea is counteracted by the increasing upper ocean temperature (Brakstad et al., 2019). Although, the effect on water density of the latter increase was smaller than that of salinity, as discussed above. Second, the Greenland Sea Water formed during convection forms only a certain fraction of the AMOC water outflow across the sills (see, for example, Hansen and Osterhus 2000; Våge et al., 2013; Saberi et al., 2020). Third, recirculation of thremohaline anomalies masks the external thermohaline forcing at decadal time scales (Eldvik et al., 2009). Finally, there are other processes, besides DC, that regulate the AMOC intensity in the North Atlantic (see, for example, a review in Buckley ad Marshall, 2016). Further studies are needed to evaluate the efficiency of this hypothetical feedback.

6. Conclusions

The main result of our study is that, during the most recent 24 years, the interannual variability in the intensity of DC in the Greenland Sea has been governed by variations of the upper ocean salinity. The latter is primarily regulated by oceanic salinity advection of the Re-circulating Atlantic Water, accumulated since the end of the previous DC season and, to a lesser extent, by winter freshwater fluxes from the melting ice. The variation of the ocean heat release to the atmosphere due to its barring by the ice cover becomes important episodically, for the winters with anomalously large and persistent Odden ice tongue (as during the winter of 1997). Therefore, ocean advection has multiple effects on the intensity of deep convection in the Greenland Sea (see also Kovalevsky and Bashmachnikov, 2020).

Therefore, depending on the time scales different combinations of major factors govern the DC. The climatic location with the most frequent and intense DC in the central Greenland Sea is a result of a combined effect of the isopycnal rise and intensity of the winter heat loss of the upper ocean. In this study we find that the long-term interannual variations of the DC intensity, at least during the study period, are primarily linked to the ocean advection, in particular to the freshwater advection. The synoptic and seasonal variability of the DC intensity should be strongly influenced by the ocean heat release to the atmosphere, as noted before (Visbeck et al., 1996; Kovalevsky et al., 2020), however this was out of the scope of this study.

7. The Supplement

7.1 Notations used in the text

$MMLD^*$ and $MMLD$ – the maximum mixed layer depth and the normalized values of $MMLD^*$, respectively

S^*_{800} and S_{800} – the area over which the DC exceeds 800 m and the normalized values of S^*_{800}, respectively

RB – the radiation balance, which is net shortwave (solar) and net longwave radiative fluxes

Q_{atm} – the sum of sensible and latent heat fluxes to the ocean

dQ_{ilid} – the difference between the turbulent heat fluxes over the ocean with no sea-ice and over the ocean with the observed ice cover (Q_{atm})

Q_{adv} – the heat convergence by oceanic advection in the layer 0-500 m

Q_{adv1} – the heat convergence by oceanic advection in the layer 500-1000 m

Q_{adv2} – the heat convergence by oceanic advection in the layer 0-1000 m

$dQ_{adv} = dQ_{adv}/dz$ – the vertical gradient of Q_{adv} in the upper 500-m layer (up-low)

FW_{PE} – the precipitation minus evaporation

FW_{ice} – the freshwater flux from the sea ice

FW_{Green} – the freshwater flux from the Greenland Ice Sheet in the Greenland Sea (between 73°N and the Fram Strait)

FW_{adv} – the freshwater convergence by oceanic advection in the layer 0-500 m

FW_{adv1} – the freshwater convergence by oceanic advection in the layer 500-1000 m

FW_{adv2} – the freshwater convergence by oceanic advection in the layer 0--1000 m

$dFW_{adv} = dFW_{adv}/dz$ – the vertical gradient of FW_{adv} in the upper 500-m layer (up-low)

α= 0.37 10^{-4} $^{o}C^{-1}$ – the coefficients of the thermal expansion

β=7.74 10^{-4} – the coefficients of the salt contraction

All fluxes above are positive when heat (freshwater) is directed into the study region.

7.2 Comparison of ARMOR results with GLORYS and SODA ocean reanalyses

Figure S1 presents the dependence between the $MMLD^*$ and S^*_{800}, derived from the data assimilating ocean general circulation models GLORYS and SODA. GLORYS has 1/12° spatial resolution, and the daily fields were averaged to monthly values. The reanalysis is based on LIM2 EVP NEMO 3.1, with an active ice block. SODA has 1/2° spatial grid and monthly-mean fields. The reanalysis is based on MOM5 ocean model and SIS1 active ice model. We used the SODA version, forced by ERA-Interim atmospheric reanalysis. Both ocean models assimilate satellite information for sea-surface temperature and salinity, as well as vertical temperature and salinity profiles. SODA additionally assimilates data from ocean moorings, while GLORYS assimilates the absolute dynamic topography from the satellite altimetry.

Both models show a higher maximum MLD of about 2500-3000 m (Fig. S1), compared to 1500 m in ARMOR, which is due to a weaker stratification and a higher variability of the low-stratified Greenland Sea Deep Water in the model results. However, the interannual and inter-monthly variations of the $MMLD^*$ (and of S^*_{800}) in the models present similar long-term tendencies for the DC intensification from mid-1990s to the end of 2000s, as in ARMOR. The correlation coefficient for the monthly $MMLD^*$and for the monthly S^*_{800} over the 96 winter months are: ARMOR- GLORYS 0.50 and 0.76, ARMOR-SODA 0.31 and 0.15, GLORYS-SODA 0.42 and 0.37, respectively. Using K-mean cluster analysis the data were split into 3 clusters with moderate, intermediate and high DC intensity (Fig. S1). For GLORYS more than 65% of the monthly points in $MMLD^*$- S^*_{800} space belong to the same clusters, as for ARMOR data. The results show that ARMOR and GLORYS show very similar interannual and inter-monthly variations, although the details of the both differ from those in SODA.

All data-sets show the similar logarithmic dependence between S^*_{800} and $MMLD^*$, differing mostly in the amplitude parameters:

ARMOR: $MMLD^* = 44.5 * (\ln(S^*_{800} + 72.8))^{3/2}$; R^2=0.47;

GLORYS: $MMLD^* = 67.9 * (\ln(S^*_{800} + 84.7))^{3/2}$; R^2=0.53;

SODA: $MMLD^* = 71.7 * (\ln(S^*_{800} + 41.2))^{3/2}$; R^2=0.48;

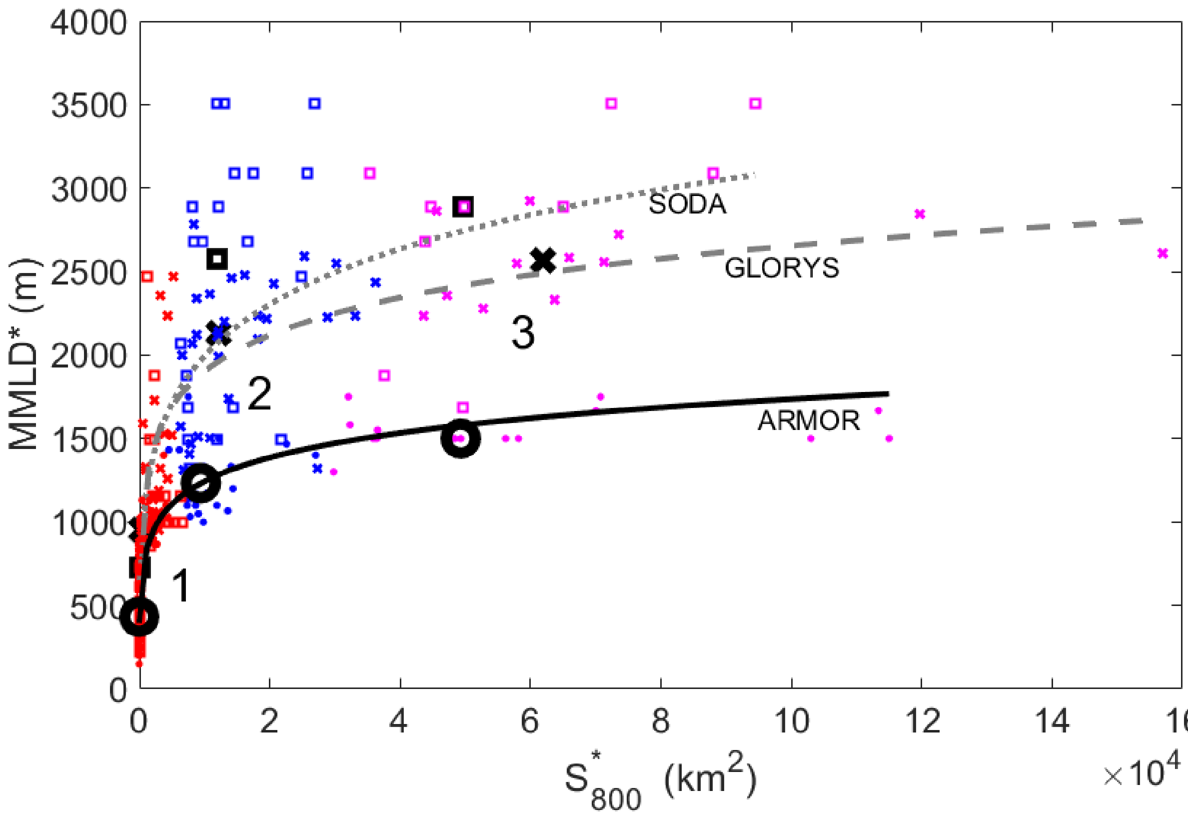

Figure S1. Cluster analysis for monthly maximum mixed layer depth ($MMLD^*$) and the square of the area with MLD over 800 m (S^*_{800}): ARMOR3D – dots, GLORYS – crosses and SODA – squares. Cluster 1 – red, cluster 2 – blue, cluster 3 – magenta. The logarithmic approximations are overlaid. The cluster centroids for each of the data-set are marked with the corresponding marker.

<u>*7.3 Spatial distributions of sea-surface fluxes in the Greenland Sea*</u>

The mean spatial distributions of heat and freshwater fluxes through the sea-surface, averaged over all the DC seasons (January to April), show an increase of the sensible and latent heat fluxes ($|Q_{atm}|$) in the north of the region and seawards of the Greenland shelf (Fig. S2a), supporting the previously suggested link between the intensity of Q_{atm} and the presence of the warmer Recirculating Atlantic Water. The effect of the ice lid in shaping the heat fluxes to the atmosphere (dQ_{ilid}) for an average winter is concentrated along the Greenland shelf and only marginally affecting the DC region (Fig. S2b). However, for some years, an anomalous ice extent (Odden ice tongue) may affect the DC intensity. The winter RB is negative, dominated by the long-wave radiation from the ocean surface (Fig. S2c). Similar to $|Q_{atm}|$, it increases north-eastwards, towards the warmer water and away from the typical DC areas.

The freshwater from ice melt (FW_{ice}) is observed only in the western part of the DC region and is mostly positive even during winter (Fig. S2d). Together with dQ_{ilid}, it should inhibit DC in the western part of the DC region. This explains why the DC is most often observed in the central and eastern parts of the Greenland Basin. However, it is not clear to what degree FW_{ice} influences the eastern areas with the most frequent DC. FW_{PE} is positive over the whole region (Fig. S2e, precipitation exceeds evaporation). Although its peak values at all grid-points are negligibly small compared to FW_{ice}, when averaged over the whole region, the inputs of both fluxes in the freshwater balance are of the same order of magnitude (Figs. 3b, 7).

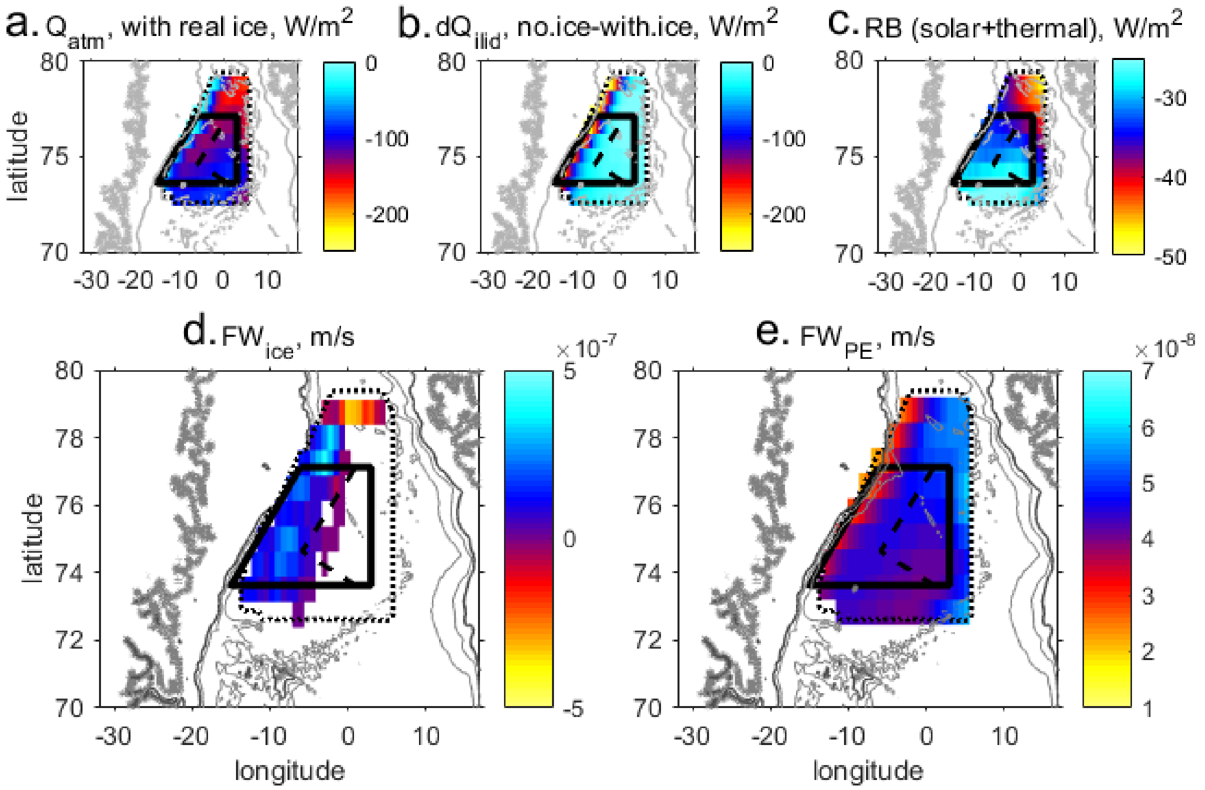

Fig. S2. The spatial distributions of heat fluxes (a-c, W m^{-2}, positive – to the ocean) and of freshwater fluxes (d-e, m s^{-1}, positive – to the ocean), averaged over the DC season (January to April)of the study period: a) sensible and latent heat fluxes with realistic ice cover from NSIDC; b) the same as (a), but with ice cover artificially removed; c)heat flux from the radiation balance (short and long wave); d) the freshwater flux from melting/forming sea ice; e) the freshwater input from precipitation minus evaporation. The positive fluxes lead to an increase of the upper ocean stratification. Black solid quadrangles mark the study region, where the DC was observed, dashed line limit from the west the region with the most frequent DC events. Grey lines are 500-m and 2500-m isobaths.

7.4 On the inverse dependence of the MMLD with the RB and Q_{atm}

Correlations of Q_{atm} and RB with the $MMLD$ are negative and significant, which is counterintuitive. We suppose that these correlations are induced and linked to the positive correlation of Q_{atm} with Q_{adv}.

The negative interannual correlations of the $MMLD$ with Q_{atm} can be, at least partly, induced by the interannual variability of Q_{adv}. Winter correlations between Q_{atm} and Q_{adv} are positive and significant (0.6-0.7). The decadal linear variations of Q_{atm} decrease (in their absolute value) together with an increase of Q_{adv}, mostly explain their correlation with the $MMLD$ (Fig.

6a,c). In the region of interest, a relatively modest increase of the air temperature and humidity, together with a certain decrease of the wind speed, compensates the SST increase and leads to a winter decrease of the area-mean $|Q_{atm}|$ (Fig. S3). The same trends are observed in the annual means (not shown). In the study region, the air temperature increases not only due to the heat flux from the ocean, but also due to a decrease of the northerly winds (Fig. S3b), as well as due to a much stronger upwind air warming in the Fram Strait (Fig. S3a), which, at least partly, is supposed to be a result of the RAW warming west of Spitsbergen.

The negative interannual correlations of the $MMLD$ with the weakly varying RB is induced by the high correlation of RB with Q_{atm} (0.7-0.8). The latter correlation is presumably a result of a conjunction of wind speed (affecting sensible and latent heat fluxes) with cloud cover (affecting short and long-wave radiation balances).

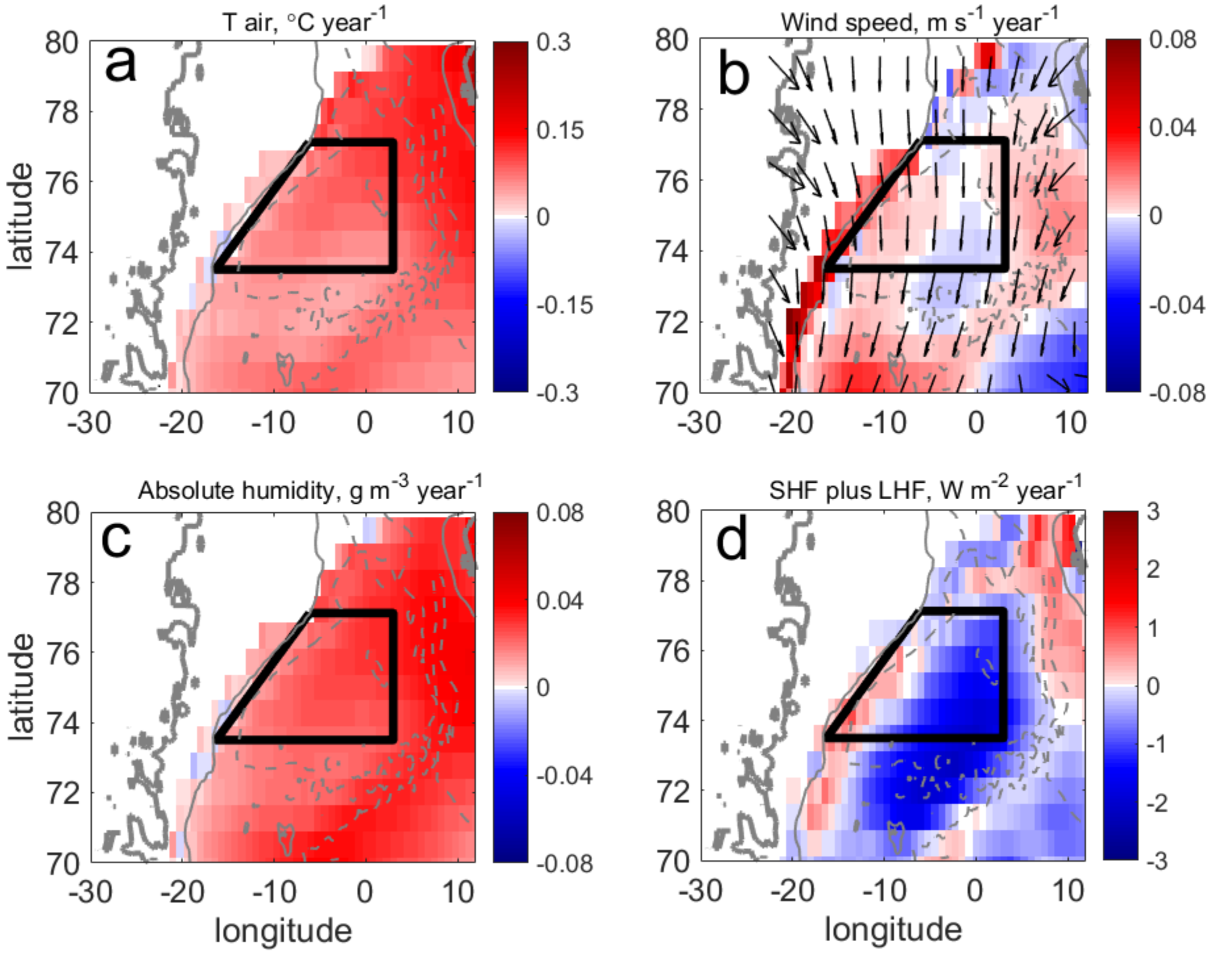

Fig. S3. Winter (January to April) linear trends (1993-2016) in: (a) the air temperature (°C year^{-1}); (b) the wind speed (m s^{-1} year^{-1}) with the mean winter wind vectors overlaid; (c) the absolute humidity (kg m^{-3} year^{-1}); (d) absolute value of the sum of sensible and latent heat fluxes (W m^{-2} year^{-1}, positive is from the ocean);. Black solid quadrangles mark the study region with the most frequent DC events. Grey lines are 500-m and 2500-m isobaths.

7.5 On the dependence of the FW_{ice} on Q_{adv} and dFW_{adv}

The positive and significant correlation of FW_{ice} with the ocean heat advection in the upper 100-m in the sea (0.45) is explained as follows. Most of the sea ice in the Greenland Sea is advected from the Arctic. Nearly all this ice melts in the Greenland Sea, as the ice volume leaving the Greenland Sea through the Denmark Strait is only 10% of that coming through the

Fram Strait (in all seasons). The FW_{ice} depends on the sea ice volume entering through the Fram Strait and on the amount of heat locally transmitted to the ice by the ocean and the atmosphere. The first factor is a function of the wind speed and direction (Germe et al., 2011). The long-term variations of the second factor primarily depends on the intensity of the oceanic heat advection (Selyuzhenok et al., 2020). In Selyuzhenok et al. (2020) it has been also noted, that increasing ice transport through the Fram Strait is observed together with an increase in the oceanic heat advection into the Greenland Sea with the RAW from the WSC (see also Fig. 5).

Winter FW_{ice} is also positively correlated with the degree of instability of the upper part of the water column (dFW_{adv}) with the correlation coefficient of 0.50. This can be explained as follows. The vertical gradient of the FW_{adv} in the upper 500-m layer (dFW_{adv}) is always negative (Figs. 3 and 7), i.e. the convergence of the oceanic freshwater advection also destabilizes the upper 500 m of the water column. Already when entering the study region, Q_{atm} continues to effectively remove the sea-surface heat from the ocean, intensifying the vertical mixing. Therefore, an increase FW_{adv} corresponds to an increase in the haline vertical mixing which uplifts warm Atlantic water from below and intensifies the sea ice melt (see also Selyuzhenok et al., 2020).

7.6 Northern and southern sections of the study region

The northern and the southern boundaries of the study region are selected to limit the area with the most frequent DC development (Fig. 1). The western boundary of the section passes along the Greenland shelf-break. The topographically trapped southwards shelf-break branch of the EGC is seen in the left parts of Figs. 1 and S4 (a,c). The eastern boundary is limited by the northwards Norwegian Atlantic Front Current (Fig. 1 and grey solid lines in Fig.S4). In the western parts of the northern and the southern sections (50-200 m), the southwards flowing warmer Atlantic water, coming from the recirculation in the Fram Strait is seen (Fig. S4). The southern section shows numerous northwards recirculations bring water from the coastally trapped current into the DC region. The oceanic advection of heat (Q_{adv}) and freshwater (FW_{adv}) is computed along these sections.

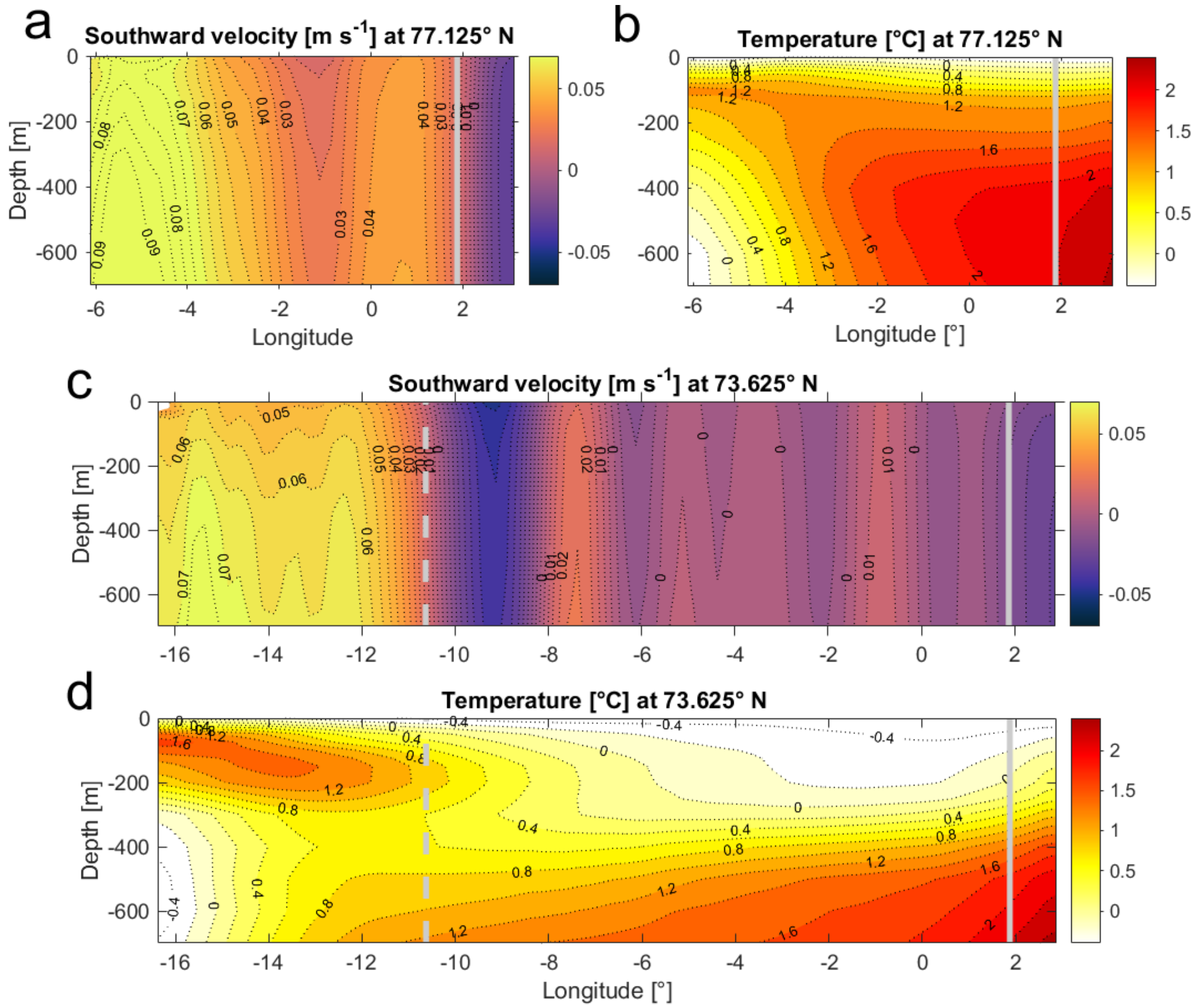

Fig. S4. Time-mean southwards current velocity (m s^{-1}, panels a, c) and water temperature (^{o}C, panels b, d) across the northern (a-b) and the southern (c-d) sections, limiting the study region. The dashed grey lines mark the time-mean eastern limit of the EGC and of the Atlantic water recirculation (for the northwards section this is also the eastern edge of the section). The solid grey lines mark the eastern edges of the sections.

7.7 A relative importance of the heat and freshwater fluxes in the density flux into the Greenland Sea

The month-to-month water density advection in the study region (Fig. S5) shows a pronounced inverse dependence with the oceanic freshwater flux (with the correlation coefficient of -0.77), while it is practically independent of the oceanic heat flux (the correlation coefficient is -0.12). The Q_{adv} weakly influences the upper ocean density as it is effectively removed by Q_{atm} already in the northern part of the region and goes to the sea ice melt (5 mSv of the melted ice corresponds to extraction of 1.5 TW of heat).

A negative (though insignificant) correlation of Q_{adv} with the DC intensity, derived in Section 4.3, therefore results from an increase of upper ocean density when a larger portion of the RAW (warmer, but what is more important – more saline) enters the study region.

Table 4 provides the budgets of the density fluxes, formed by the corresponding heat fluxes (Table 2) and freshwater fluxes (Table 3). The results show an overall higher effect of salinity of the variability of density fluxes into the upper Greenland Sea.

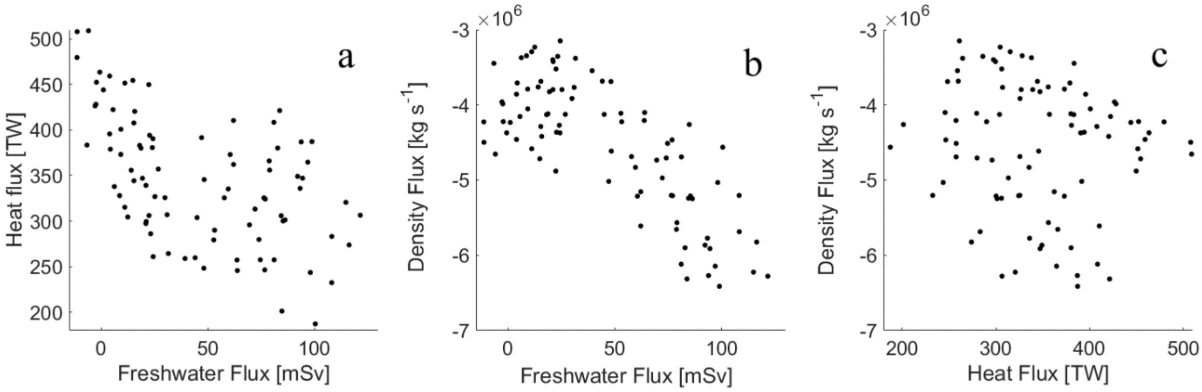

Fig. S5. Scatter diagrams of the oceanic advective fluxes through 77.1°N, averaged over the upper 500-m layer and accumulated since August of the previous year to the months in the DC season (January-April): (a) the heat advection versus the freshwater advection, (b) the density advection versus the freshwater advection, (c) the density advection versus the heat advection.

Table 4. Upper ocean mean water density fluxes and their standard deviations at interannual time scales (*10^3 kg m^{-3} s^{-1}) estimated from heat fluxes (DF_{RB} – from the radiation balance, DF_{atm} – from the ocean-atmosphere heat exchange, $DF_{T.adv}$ – from the oceanic heat advection in the upper 500m layer) and from freshwater fluxes (DF_{PE} – from the precipitation minus evaporation, DF_{ice} – from the ice melt minus ice formation at the sea-surface, $DF_{S.adv}$ – from the oceanic freshwater advection in the upper 500m layer). See Tables 2 and 3 and Eqs.3-6. The global means are computed from the 3-year smoothed seasonal means for the pre-DC season (June to December) and the DC season (January to April). The fluxes are to the ocean, positive values means a water density increase.

From heat fluxes	DF_T, pre-DC season	DF_T, DC season	From freshwater fluxes	DF_S, pre-DC season	DF_S , DC season
DF_{RB} (to the ocean)	-37 ±6	42 ±5	DF_{PE}	-124 ±14	-167 ±30
DF_{atm} (to the ocean)	94 ±14	146 ±34	DF_{ice}	-138 ±51	-243 ±170
$DF_{T.adv}$(0-500 m)	-30 ±32	-14 ±52	$DF_{S.adv}$(0-500 m)	122 ±62	119 ±65
DF_{RB}+$DF_{atm} + DF_{adv}$	28 ±53	174 ±90	$DF_{PE} + DF_{ice} + DF$	-140 ±127	-292 ±265

Acknowledgement: The research was founded by Saint Petersburg State University (project N 75295423). D.S. Dukhovskoy was funded by the DOE (award DE-SC0014378).

References

1. Alekseev G.V., Ivanov V.V., Korablev A.A. 1994. Interannual variability of the thermohaline structure in the convective gyre of the Greenland Sea. The Polar Oceans and Their Role in Shaping the Global Environment. Geophys. Monogr. Ser. 85, 485-496. AGU, Washington. doi:10.1029/GM085p0485.
2. Alekseev, G.V., Bogorodskiy, P.V., Nagurny, A.P. 1989. Thermohaline structure of waters in the area with cyclonic circulation and upwelling. Structure and variability of largescale processes in the Norwegian zone of intensive ocean-atmosphere interactions (eds. Nikolayev, Yu.V., Alekseev, G.V.). Hydrometeoizdat., Leningrad. 37-43. (In Russian)

3. Alekseev, G.V., Johannessen, O.M., Kovalevsky, D. V. 2001. On development of convective motions under the influence of local density perturbations on the sea surface. Izvestiya RAS. Atmospheric and ocean physics. 37 (3), 368-377. (In Russian)

4. Alekseev, G. V., Johannessen, O. M., Korablev, A. A., Ivanov, V. V., Kovalevsky, D. V. 2001. Interannual variability in water masses in the Greenland Sea and adjacent areas. Polar Research. 20 (2), 201-208. https://doi.org/10.1111/j.1751-8369.2001.tb00057.x.

5. Androsov, A., Rubino, A., Romeiser, R., Sein, D. V. 2005. Open-ocean convection in the Greenland Sea: preconditioning through a mesoscale chimney and detectability in SAR imagery studied with a hierarchy of nested numerical models. Meteorologische Zeitschrift. 14 (6), 693-702. https://doi.org/10.1127/0941-2948/2005/0078.

6. Arbic, B. K., Scott, R. B., Chelton, D. B., Richman, J. G., Shriver, J. F. 2012. Effects of stencil width on surface ocean geostrophic velocity and vorticity estimation from gridded satellite altimeter data. J. Geophys. Res. 117, C03029. doi:10.1029/2011JC007367.

7. Arthur, D., Vassilvitskii, S. 2007. **k**-means++: the advantages of careful seeding. Proceedings of the Eighteenth Annual ACM-SIAM Symposium on Discrete Algorithms. 1027–1035.

8. Aubert, O., Le Bars, M., Le Gal, P., Marcus, P. S. 2012. The universal aspect ratio of vortices in rotating stratified flows: experiments and observations. Journal of Fluid Mechanics, 706, 34-45. https://doi.org/10.1017/jfm.2012.176.

9. Azetsu-Scott, K., Jones, E. P., Gershey, R. M. 2005. Distribution and ventilation of water masses in the Labrador Sea inferred from CFCs and carbon tetrachloride. Marine chemistry, 94 (1), 55-66. https://doi.org/10.1016/j.marchem.2004.07.015.

10. Bamber, J., den Broeke, M., Ettema, J., Lenaerts, J., Rignot, E. 2012. Recent large increases in freshwater fluxes from Greenland into the North Atlantic. Geophys. Res. Lett. 39, L19501, doi:10.1029/2012GL052552.

11. Bamber J.L., Tedstone, A.J., King, M.D., Howat, I.M., Enderlin, E.M., van den Broeke, M.R., Noel, B. 2018. Land ice freshwater budget of the Arctic and North Atlantic Oceans: 1. Data, methods, and results. Journal of Geophysical Research: Oceans, 123 (3), 1827-1837

12. Bashmachnikov, I. L, Fedorov, A. M., Vesman, A. V., Belonenko, T. V., Koldunov, A. V., Dukhovskoy, D. S. 2018. Thermohaline convection in the subpolar seas of the North Atlantic from satellite and in situ observations. Part 1: Localization of the deep convection sites. Sovremennye Problemy Distantsionnogo Zondirovaniya Zemli iz Kosmosa. 15 (7), 184–194.doi: 10.21046/2070-7401-2018-15-7-184-194. (In Russian)

13. Bashmachnikov, I. L, Fedorov, A. M., Vesman, A. V., Belonenko, T. V., Dukhovskoy, D. S. 2019. Thermohaline convection in the subpolar seas of the North Atlantic from satellite and in situ observations. Part 2: indices of intensity of deep convection. Sovremennye Problemy Distantsionnogo Zondirovaniya Zemli iz Kosmosa. 16 (1), 191–201.doi: 10.21046/2070-7401-2019-16-1-191-201. (In Russian)

14. Bashmachnikov, I., Nascimento A., Neves F., Calheiros T., Koldunov N.V., 2015a. Distribution of Intermediate Water Masses in the Subtropical Northeast Atlantic. Ocean Science. 11, 803-827. doi:10.5194/os-11-803-2015.

15. Bashmachnikov, I., Neves F., Calheiros T., Carton X., 2015b. Properties and pathways of Mediterranean water eddies in the Atlantic. Progress in Oceanography. 137A, 149-172. doi:10.1016/j.pocean.2015.06.001.

16. Bashmachnikov, I., Sokolovskiy M.A., Belonenko T.V., Volkov D.L., Isachsen P.E. Carton X. 2017. On the vertical structure and stability of the Lofoten vortex in the Norwegian Sea. Deep-Sea Research I. 128, 1-27 https://doi.org/10.1016/j.dsr.2017.08.001

17. Bashmachnikov., I.L., Volkov, D.L., Yurova, A.Yu., Bobylev L.P., 2016a. Interannual variability of oceanic heat fluxes in the Atlantic Sector of the Arctic Ocean, U Arctic Congress, 12-16 of September. St.Petersburg, Russia

18. Berry, D. I., Kent, E. C. 2009. A new air–sea interaction gridded dataset from ICOADS with uncertainty estimates. Bulletin of the American Meteorological Society, 90(5), 645-656.

19. Beszczynska-Möller A., von Appen W.-J., Fahrbach E. 2015. Physical oceanography and current meter data from moorings F1-F14 and F15/F16 in the Fram Strait, 1997-2012. PANGAEA. doi:10.1594/PANGAEA.150016.
20. Beszczynska-Möller, A., Fahrbach E., Schauer U., Hansen E. 2012. Variability in Atlantic water temperature and transport at the entrance to the Arctic Ocean, 1997–2010. ICES Journal of Marine Science. 69 (5), 852–863. https://doi.org/10.1093/icesjms/fss056.
21. Björk, G., Gustafsson, B. G., Stigebr and t, A. 2001. Upper layer circulation of the Nordic seas as inferred from the spatial distribution of heat and freshwater content and potential energy. Polar research. 20 (2), 161-168. https://doi.org/10.1111/j.1751-8369.2001.tb00052.x.
22. Boning, C. W., Behrens, E., Biastoch, A., Getzlaff, K., Bamber, J. L. 2016. Emerging impact of Greenland meltwater on deepwater formation in the North Atlantic Ocean. Nature Geoscience. volume 9, pages 523–527.
23. Bonisch, G., Blindheim, J., Bullister, J. L., Schlosser, P. Wallace, D. W. R. 1997. Long-term trends of temperature, salinity, density and transient tracers in the central Greenland Sea. J. Geophys. Res. 102(C8), 18553– 18571. doi:10.1029/97JC00740.
24. Born, A., Stocker, T. F., Raible, C. C., Levermann, A. 2013. Is the Atlantic subpolar gyre bistable in comprehensive coupled climate models? Climate dynamics. 40(11-12). 2993-3007.
25. Box, J. E., Bromwich, D. H., Bai, L. S. 2004. Greenland ice sheet surface mass balance 1991–2000: Application of Polar MM5 mesoscale model and in situ data. Journal of Geophysical Research: Atmospheres. 109, D16105. doi:10.1029/2003JD004451.
26. Bower A. S., von Appen W. J. 2008. Interannual variability in the pathways of the North Atlantic Current over the Mid-Atlantic Ridge and the impact of topography, Journal of Physical Oceanography. 38(1).104-120
27. Broecker, W. S., 1987. The biggest chill. Natural History 97 (2): pp. 74-82
28. Broecker, W. S., 1991. The great ocean conveyor. Oceanography, 4(2), 79-89.
29. Brakstad, A., Våge, K., Håvik, L., Moore, G.W.K., 2019. Water mass transformation in the Greenland Sea during the period 1986–2016. Journal of Physical Oceanography, 49(1), pp.121-140.
30. Buckley M. W., Marshall J. 2016. Observations, inferences, and mechanisms of Atlantic Meridional Overturning Circulation variability: A review. Rev. Geophys. 54, 5-63. doi:10.1002/2015RG000493.
31. Budeus G., Schneider W., Krause G. 1998. Winter convective events and bottom water warming in the Greenland Sea. J. Geophys. Res. 103 (C9), 18513– 18527. doi:10.1029/98JC01563.
32. Budeus G., Schneider W., Krause G. 1998. Winter convective events and bottom water warming in the Greenland Sea. J. Geophys. Res. 103 (C9), 18513– 18527. doi:10.1029/98JC01563.
33. Chafik, L., Nilsson, J., Skagseth, O., Lundberg, P. (2015). On the flow of Atlantic water and temperature anomalies in the Nordic Seas toward the Arctic Ocean. Journal of Geophysical Research: Oceans, 120(12), 7897-7918.
34. Chafik, L., Rossby, T. 2019. Volume, heat, and freshwater divergences in the subpolar North Atlantic suggest the Nordic seas as key to the state of the meridional overturning circulation. Geophysical Research Letters, 46(9), 4799-4808.
35. Chatterjee, S., Raj, R.P., Bertino, L., Skagseth, Ø., Ravichandran, M., Johannessen, O.M., 2018. Role of Greenland Sea gyre circulation on Atlantic water temperature variability in the Fram Strait. Geophysical Research Letters, 45 (16), pp.8399-8406.
36. Chen, X., Tung, K. K. 2018. Global surface warming enhanced by weak Atlantic overturning circulation. Nature, 559(7714), 387-391.
37. Chu, S., Gascard, J. C. 1991. Deep convection and deep water formation in the oceans. 57. Elsevier.

38. Clarke, R. A., J.-C. Gascard, 1983: The formation of Labrador Sea water. Part 1: Large-scale processes. J. Phys. Oceanogr., 13, 1764-1788.

39. Clarke, A., Swift, J. H., Reid, J.C., Koltermann, K. P. 1990. The formation of the Greenland Sea Deep Water: double diffusion or deep convection. Deep-Sea Res. 37, 1385-1424. https://doi.org/10.1016/0198-0149(90)90135-I.

40. Comiso, J. C., Wadhams, P., Pedersen, L. T., Gersten, R. A.2001. Seasonal and interannual variability of the Odden ice tongue and a study of environmental effects. J. Geophys. Res. 106(C5), 9093– 9116. doi:10.1029/2000JC000204.

41. Condron, A., Renfrew, I.A. 2013. The impact of polar mesoscale storms on northeast Atlantic Ocean circulation. Nature Geoscience. 6(1), pp.34-37.

42. Curry, R., Mauritzen, C. 2005. Dilution of the northern North Atlantic Ocean in recent decades. Science. 308 (5729), 1772-1774. doi: 10.1126/science.1109477

43. de Boyer Montégut, C., Madec, G., Fischer, A. S., Lazar, A., Iudicone, D. 2004. Mixed layer depth over the global ocean: An examination of profile data and a profile-based climatology. Journal of Geophysical Research: Oceans. 109, C12003. doi:10.1029/2004JC002378.

44. de Steur L., Hansen E., Gerdes R., Karcher M., Fahrbach E., Holfort J. 2009. Freshwater fluxes in the East Greenland Current: A decade of observations. Geophysical Research Letters. 36 (23). L23611.doi: 10.1029/2009GL041278.

45. Dee, D. and National Center for Atmospheric Research Staff (Eds). Last modified 11 Nov 2016. "The Climate Data Guide: ERA-Interim." https://climatedataguide.ucar.edu/climate-data/era-interim.

46. Deshayes, J., Curry, R., Msadek, R. 2014. CMIP5 model inter-comparison of freshwater budget and circulation in the North Atlantic. Journal of Climate, 27 (9), 3298-3317. https://doi.org/10.1175/JCLI-D-12-00700.1

47. Dickson, R.R., Meincke, J., Rhines, P. 2008. Arctic, Sub-arctic Ocean Fluxes: Defining the Role of the Northern Seas in Climate. Springer, p. 736.

48. Drange, H., Dokken, T., Furevik, T., Gerdes, R., Berger, W., Nesje, A., Østerhus, S. 2005. The Nordic seas: an overview. American Geophysical Union. 1-10.

49. Drijfhout, S. 2015. Competition between global warming and an abrupt collapse of the AMOC in Earth's energy imbalance. Scientific reports. 5, 14877. doi: 10.1038/srep14877

50. Dukhovskoy, D. S., Johnson, M. A., Proshutinsky, A. 2004. Arctic decadal variability: An auto-oscillatory system of heat and fresh water exchange. Geophys. Res. Lett. 31, L03302. doi:10.1029/2003GL019023.

51. Dukhovskoy D.S. et al. 2016. Greenland freshwater pathways in the sub-Arctic Seas from model experiments with passive tracers. J. Geophys. Res. Oceans. 121. 877–907. doi:10.1002/2015JC011290

52. Dukhovskoy, D. S., Bourassa, M. A., Petersen, G. N., and Steffen, J. (2017), Comparison of the ocean surface vector winds from atmospheric reanalysis and scatterometer-based wind products over the Nordic Seas and the northern North Atlantic and their application for ocean modeling, J. Geophys. Res. Oceans, 122, 1943– 1973, doi:10.1002/2016JC012453.

53. Dukhovskoy, D. S., Yashayaev, I., Proshutinsky, A., Bamber, J. L., Bashmachnikov, I. L., Chassignet, E. P., et al. 2019. Role of Greenland freshwater anomaly in the recent freshening of the subpolar North Atlantic. Journal of Geophysical Research: Oceans. 124, 3333–3360. https://doi.org/10.1029/2018JC014686.

54. Eldevik, T., Nilsen, J. E. Ø., Iovino, D., Olsson, K. A., Sandø, A. B., Drange, H. 2009. Observed sources and variability of Nordic seas overflow. Nature Geoscience, 2(6), 406-410.

55. Fairall, C. W., Bradley, E. F., Hare, J. E., Grachev, A. A., Edson, J. B., 2003. Bulk parameterization of air–sea fluxes: Updates and verification for the COARE algorithm. Journal of climate, 16(4), 571-591.

56. Falina, A.S., Sarafanov, A.A. 2015. On the formation of the lower limb of the North Atlantic Meridional Overturning Circulation. Doklady. Earth Sciences. 461 (2), 427-431. (In Russian)

57. Falina, A.S., Sarafanov, A.A., Dobrolyubov, S.A., Zapotyilko, V.S., Gladyishev, S.V. 2017. Convection and water stratification in the North Atlantic ocean according to measurements in winter 2013/14. Vestnik Moskovskogo universiteta. Ser. 5: Geografiya. 4, 45-54. (In Russian)

58. Falina, A.S., Sarafanov, A.A., Sokov, A.V., 2007. On the renewal of Labrador Sea water in the Irminger basin. Oceanology, 47(4), 494-499.

59. Ferreira, D., Cessi, P., Coxall, H.K., De Boer, A., Dijkstra, H. A., Drijfhout, S. S., ..., Wills, R.C. (2018). Atlantic-Pacific asymmetry in deep water formation. Annual Review of Earth and Planetary Sciences, 46 (1), 327-352

60. Fedorov, A.M., Bashmachnikov, I.L, Belonenko, T.V. 2018. Localization of areas of deep convection in the Nordic seas, the Labrador Sea and the Irminger Sea. Vestnik of Saint Petersburg University. Earth Sciences. 63 (3), 345–362. https://doi.org/10.21638/spbu07.2018.306. (In Russian)

61. Fedorov, A.M., Bashmachnikov, I.L. 2020. Quality assessments of the deep convection intensity for a limited number of in-situ measurements. Dynamics of Atmospheres and Oceans (submitted)

62. Fischer J., Schott F., Visbeck M.1995 Greenland Sea convection monitoring. In: The Nordic Seas, Humburg, March 7-9, 1995. p.61-64.

63. Frolov, I.E., Gudkovich, Z.M., Karlin, V.P., Kovalev E.G., Smolyanitsky, V.M. 2007. Scientific researches in Arctic. Volume 2. Climatic changes in the ice cover of the Eurasian shelf seas. Nauka. Saint-Petersburg. pp. 136. (In Russian)

64. Furevik, T., Bentsen, M., Drange, H., Johannessen, J. A., Korablev, A. 2002. Temporal and spatial variability of the sea surface salinity in the Nordic Seas. Journal of Geophysical Research: Oceans, 107(C12), SRF-10.

65. Ghaffari, P., Isachsen, P. E., Nost, O. A., Weber, J. E., 2018. The influence of topography on the stability of the Norwegian Atlantic Current off northern Norway. Journal of Physical Oceanography, 48(11), 2761-2777.

66. Garzoli, S. L., Matano, R. 2011. The South Atlantic and the Atlantic meridional overturning circulation. Deep Sea Research Part II: Topical Studies in Oceanography. 58 (17), 1837-1847. https://doi.org/10.1016/j.dsr2.2010.10.063

67. Gascard, J. C., Watson, A. J., Messias, M. J., Olsson, K. A., Johannessen, T., Simonsen, K. 2002. Long-lived vortices as a mode of deep ventilation in the Greenland Sea. Nature. 416 (6880), 525-527.

68. Gelderloos, R., Katsman, C.A., Våge, K. 2013. Detecting Labrador Sea water formation from space. J. Geophys. Res. C: Oceans. 118 (4), 2074-2086. doi:10.1002/jgrc.20176.

69. Gerdes, R., W. Hurlin, and S. M. Griffies (2006), Sensitivity of a global ocean model to increased run-off from Greenland, Ocean Modell., 12(3–4), 416– 435.

70. Germe, A., Houssais, M.-N., Herbaut, C., Cassou, C.2011. Greenland Sea sea-ice variability over 1979–2007 and its link to the surface atmosphere. J. Geophys. Res. 116, C10034. doi:10.1029/2011JC006960.

71. Giles, K. A., Laxon, S. W., Ridout, A. L., Wingham, D. J., Bacon, S. 2012. Western Arctic Ocean freshwater storage increased by wind-driven spin-up of the Beaufort Gyre. Nature Geoscience. 5 (3), 194-197.

72. Gladyshev, S. V., Gladyshev, V. S., Falina, A. S., Sarafanov, A. A. 2016. Winter convection in the Irminger Sea in 2004–2014. Oceanology. 56 (3), 326-335. doi: 10.1134/S0001437016030073.

73. Glessmer, M. S., Eldevik, T., Våge, K., Nilsen, J. E. Ø., Behrens, E. 2014. Atlantic origin of observed and modelled freshwater anomalies in the Nordic Seas. Nature Geoscience. 7 (11), 801-805.

74. Golubkin, P., Smirnova, J., and Bobylev, L. 2021. Satellite-Derived Spatio-Temporal Distribution and Parameters of North Atlantic Polar Lows for 2015–2017. Atmosphere, 12(2), 224. https://doi.org/10.3390/atmos12020224.
75. GSP Group. 1990. Greenland Sea Project - a venture toward improved understanding of the ocean's role in climate. Eos Trans. AGU. 71 (24), 750–756. doi:10.1029/90EO00208.
76. Gudkovich Z.M., Nikolaeva A.Ya. 1963. Sea ice drift in the Arctic basin and its link to ice volume in the Arctic seas of the USSR. Trudy AARI. 104, 210. (In Russian)
77. Guinehut, S., Dhomps, A.L., Larnicol, G., Le Traon, P.-Y. 2012. High resolution 3-D temperature and salinity fields derived from in situ and satellite observations. Ocean Sci. 8, 845-857. https://doi.org/10.5194/os-8-845-2012.
78. Guinehut, S., Le Traon, P.-Y.,Larnicol, G., Philipps, S. 2004. Combining Argo and remote-sensing data to estimate the ocean three-dimensional temperature fields—a first approach based on simulated observations Journal of Marine Systems. 46 (1–4), 85-98. https://doi.org/10.1016/j.jmarsys.2003.11.022.
79. Gulev S.K., Kattsov V.M., Solomina O.N. Global warming continues. Herald of the Russian Academy of Sciences. 78 (1), 44–50.
80. Gulev, S., Jung T., Ruprecht E. 2007a. Estimation of the Impact of Sampling Errors in the VOS Observations on Air–Sea Fluxes. Part I: Uncertainties in Climate Means. J. Climate. 20, 279–301. https://doi.org/10.1175/JCLI4010.1.
81. Gulev, S., Jung T., Ruprecht E. 2007b. Estimation of the Impact of Sampling Errors in the VOS Observations on Air–Sea Fluxes. Part II: Impact on Trends and Interannual Variability. J. Climate. 20, 302–315. https://doi.org/10.1175/JCLI4008.1.
82. Hakkinen, S., and Rhines, P. B. (2009). Shifting surface currents in the northern North Atlantic Ocean. Journal of Geophysical Research: Oceans, 114(C4), C04005, doi:10.1029/2008JC004883
83. Hansen, E., Gerland, S., Granskog, M.A., Pavlova, O., Renner, A.H.H., Haapala, J., Løyning, T.B. and Tschudi, M. 2013. Thinning of Arctic sea ice observed in Fram Strait: 1990–2011. Journal of Geophysical Research: Oceans. 118 (10), 5202-5221. doi:10.1002/jgrc.20393.
84. Hansen B., Osterhus S. 2000. North Atlantic –Nordic Seas Exchanges. Progress in Oceanography, 45, 109-208.
85. Hodges, K. I., 1995. Feature tracking on the unit sphere. Monthly Weather Review, 123(12), 3458-3465.
86. Hodges, K. I. (1999). Adaptive constraints for feature tracking. Monthly Weather Review, 127(6), 1362-1373.
87. Hodges, K. I., Lee, R. W., and Bengtsson, L., 2011. A comparison of extratropical cyclones in recent reanalyses ERA-Interim, NASA MERRA, NCEP CFSR, and JRA-25. Journal of Climate, 24(18), 4888-4906.
88. Hoskins, B. J. and Hodges, K. I., 2002. New perspectives on the Northern Hemisphere winter storm tracks. Journal of the Atmospheric Sciences, 59(6), 1041-1061.
89. Herrmann, M., Bouffard, J., Béranger, K. 2009. Monitoring open-ocean deep convection from space. Geophys. Res. Lett. 36, L03606. doi:10.1029/2008GL036422.
90. Jeansson, E., Jutterström, S., Rudels, B., Anderson, L.G., Olsson, K.A., Jones, E.P., Smethie Jr, W.M. and Swift, J.H., 2008. Sources to the East Greenland Current and its contribution to the Denmark Strait Overflow. Progress in Oceanography, 78(1), 12-28.
91. Jochumsen, K., Quadfasel D., Valdimarsson H., Jonsson S. 2012. Variability of the Denmark Strait overflow: Moored time series from 1996–2011. J. Geophys. Res. 117. C12003. doi:10.1029/2012JC008244.
92. Johannessen, O.M., Johannessen J.A., Svendsen E., Shuchmann R.A., Campbell W.J., Josberger E. 1987. Ice-Edge Eddies in the Fram Strait Marginal Ice Zone. Science. 236, 427 – 429. doi: 10.1126/science.236.4800.427.

93. Johannessen, O. M., Sandven, S., Johannessen, J. A. 1991. Eddy-related winter convection in the Boreas Basin. Elsevier Oceanography Series. 57, 87-105. https://doi.org/10.1016/S0422-9894(08)70062-X.

94. Johannessen, O. M., Lygre, K., Eldevik, T. 2005. Convective chimneys and plumes in the Northern Greenland Sea. The Nordic Seas: An Integrated Perspective. 251-272. doi: 10.1029/xxxgmxx.

95. Johannessen, O. M., Korablev, A., Miles, V., Miles, M. W., Solberg, K. E. (2011). Interaction between the warm subsurface Atlantic water in the Sermilik Fjord and Helheim glacier in southeast Greenland. Surveys in geophysics, 32(4-5), 387-398

96. Johannessen, O. M., M. Babiker, M. W. Miles, 2013: Unprecedented retreat in a 50-year observational record for Petermann Glacier, North Greenland, Atmos. Oceanic Sci. Lett., 6, 259–265, doi:10.3878/j.issn. 1674-2834.13.0021

97. Johannessen, O.M., S.I. Kuzmina, L.P. Bobylev, M.W. Miles. 2016. Surface air temperature variability and trends in the Arctic: new amplification assessment and regionalization. Tellus A. 68, 28234. http://dx.doi.org/10.3402/tellusa.v68.28234.

98. Johnson, H.L., Cessi, P., Marshall, D.P., Schloesser, F., Spall, M.A. 2019. Recent contributions of theory to our understanding of the Atlantic Meridional Overturning Circulation. Journal of Geophysical Research: Oceans, 124(8), 5376-5399.

99. Jones, H., Marshall, J. 1993. Convection with rotation in a neutral ocean: A study of open-ocean deep convection. Journal of Physical Oceanography, 23(6), 1009-1039.

100. Jonsson, S., 1991. Seasonal and interannual variability of wind stress curl over the Nordic Seas. Journal of Geophysical Research: Oceans, 96(C2), pp.2649-2659.

101. Jonsson S., Valdimarsson H. 2012. Water mass transport variability to the North Icelandic shelf, 1994–2010. ICES Journal of Marine Science. 69 (5), 809–815. https://doi.org/10.1093/icesjms/fss024.

102. Josey S. A., Marsh R. Surface freshwater flux variability and recent freshening of the North Atlantic in the eastern subpolar gyre. J. Geophys. Res. 110, C05008. doi:10.1029/2004JC002521.

103. Kara A.B., Rochford P.A., Hurlburt H.E. 2003. Mixed layer depth variability over the global ocean. J. Geophys. Res. 108, 3079. doi:10.1029/2000JC000736, C3.

104. Kawasaki, T., Hasumi, H. 2014. Effect of freshwater from the West Greenland Current on the winter deep convection in the Labrador Sea. Ocean Modelling. 75, 51-64. https://doi.org/10.1016/j.ocemod.2014.01.003.

105. Khatiwala S., Schlosser P., Visbeck M. 2002. Rates and mechanisms of water mass transformation in the Labrador Sea as inferred from tracer observations. Journal of Physical Oceanography. 32 (2), 666-686. https://doi.org/10.1175/1520-0485(2002)032<0666:RAMOWM>2.0.CO;2

106. Killworth, P. D. 1983. Deep convection in the world ocean. Reviews of Geophysics. 21 (1), 1-26.

107. Koenigk T., Mikolajewicz U., Haak H., Jungclaus J. 2007. Arctic freshwater export in the 20th and 21st centuries. J. Geophys. Res. 112, G04S41. doi:10.1029/2006JG000274.

108. Köhl, A., Serra, N. (2014). Causes of decadal changes of the freshwater content in the Arctic Ocean. Journal of Climate, 27 (9), 3461-3475. https://doi.org/10.1175/JCLI-D-13-00389.1.

109. Koszalka I., LaCasce, J.H., Andersson, M., Orvik, K.A., Mauritzen, C., 2011. Surface circulation in the Nordic Seas from clustered drifters. Deep-Sea Research I. 58. P. 468-485. doi:10.1016/j.dsr.2011.01.007.

110. Korablev, A.A., 2001. Water structure and variability of oceanographic parameters in the Norwegian and Greenland Seas. PhD thesis, Saint-Petersburg.(In Russian)

111. Kovalevsky D.V., 2002. Analysis and modelling of the deep convection in the Greenland Sea. PhD thesis, Saint-Petersburg. (In Russian)

112. Kovalevsky D.V., Bashmachnikov I.L., 2019. Nonlinear dynamics of deep open-ocean convection: an analytical approach. In: “Nonlinear Dynamics, Chaos, and Complexity II: memory of Valentin Afraimovich (1945-2018)”, Springer (accepted)

113. Kovalevsky D.V., Bashmachnikov, I.L., 2020. An analytical model of open-ocean deep convection with multiple steady states, Ocean Modelling, 154, 101680, 1-18, doi: 10.1016/j.ocemod.2020.101680

114. Kovalevsky D.V., Bashmachnikov, I.L., Alekseev, G.V. 2020. Formation and decay of a deep convective chimney, Ocean Modelling, 148, 101583, https://doi.org/10.1016/j.ocemod.2020.101583

115. Kwok, R., Cunningham, G.F. and Pang, S.S., 2004. Fram Strait sea ice outflow. Journal of Geophysical Research: Oceans. 109, C01009, doi:10.1029/2003JC001785.

116. Langehaug, H.R., Falck, E., 2012. Changes in the properties and distribution of the intermediate and deep waters in the Fram Strait. Progress in Oceanography, 96(1), pp.57-76.

117. Lappo S. S. 1984. On the mechanisms of the northwards heat advection across the equator in the Atlantic Ocean. Investigations of the process of ocean=atmosphere interactions, Moscow, 125-129 (in Russian).

118. Larnicol, G., Guinehut, S., Rio, M. H., Drevillon, M., Faugere, Y., Nicolas, G. 2006. The global observed ocean products of the French Mercator project. Proceedings of the Symposium on 15 Years of Progress in Radar Altimetry, 13–18 March 2006, Venice, Italy.

119. Lauvset, S.K., Brakstad, A., Våge, K., Olsen, A., Jeansson, E., Mork, K.A., 2018. Continued warming, salinification and oxygenation of the Greenland Sea gyre. Tellus A: Dynamic Meteorology and Oceanography, 70(1), pp.1-9.

120. Latarius, K., Quadfase, D. 2016. Water mass transformation in the deep basins of the Nordic Seas: Analyses of heat and freshwater budgets. Deep Sea Research. Part I: Oceanographic Research Papers. 114, 23-42. https://doi.org/10.1016/j.dsr.2016.04.012.

121. Lecomte, O., Fichefet, T., Vancoppenolle, M., Domine, F., Massonnet, F., Mathiot, P., ..., Barriat, P. Y. 2013. On the formulation of snow thermal conductivity in large-scale sea ice models. Journal of Advances in Modeling Earth Systems, 5(3), 542-557.

122. Lenaerts, J. T. M., Bars D. Le, van Kampenhout L., Vizcaino M., Enderlin E. M., van den Broeke M. R. 2015. Representing Greenland ice sheet freshwater fluxes in climate models. Geophys. Res. Lett. 42, 6373–6381. doi:10.1002/2015GL064738.

123. Levermann, A., Born, A. 2007. Bistability of the Atlantic subpolar gyre in a coarse-resolution climate model, Geophysical Research Letters. 34(24). L24605. doi:10.1029/2007GL031732.

124. Lien, V. S., Vikebø, F. B., Skagseth, O. (2013). One mechanism contributing to co-variability of the Atlantic inflow branches to the Arctic. Nature Communications, 4(1), 1-6.

125. Liu, C. H., Wakimoto, R. M., Roux, F. (1997). Observations of mesoscale circulations within extratropical cyclones over the North Atlantic Ocean during ERICA. Monthly weather review, 125(3), 341-364.

126. Lockwood, J. G. 2001. Abrupt and sudden climatic transitions and fluctuations: a review. International Journal of Climatology. 21 (9), 1153-1179. doi:10.1002/joc.630.

127. Lozier, M.S., Li, F., Bacon, S., Bahr, F., Bower, A.S., Cunningham, S.A., De Jong, M.F., De Steur, L., Deyoung, B., Fischer, J. and Gary, S.F., 2019. A sea change in our view of overturning in the subpolar North Atlantic. Science, 363(6426),516-521.

128. Lumpkin, R., Speer, K. 2007. Global ocean meridional overturning. J. Phys. Oceanogr. 37 (10), 2550–2562. https://doi.org/10.1175/JPO3130.1

129. Luo, H., Castelao, R. M., Rennermalm, A. K., Tedesco, M., Bracco, A., Yager, P. L., Mote, T. L. 2016. Oceanic transport of surface meltwater from the southern Greenland ice sheet. Nature Geoscience. 9, 528–532.

130. Malmberg, S.-A. 1983. Hydrographic investigations in the Iceland and Greenland Seas in late winter 1971 - "Deep Water Project", J6kull. 33, 133-140.

131. Malmberg, S.A., Jonsson, S., 1997. Timing of deep convection in the Greenland and Iceland Seas. ICES Journal of Marine Science, 54(3), pp.300-309.

132. Marnela, M., Rudels, B., Houssais, M.N., Beszczynska-Möller, A., Eriksson, P.B., 2013. Recirculation in the Fram Strait and transports of water in and north of the Fram Strait derived from CTD data. Ocean Science. 9, 499–519. doi:10.5194/os-9-499-2013.

133. Marshall, J., Schott, F. 1999. Open-ocean convection: Observations, theory, and models. Reviews of Geophysics, 37 (1), 1-64. https://doi.org/10.1029/98RG02739.

134. Maslowski, W., Kinney, J.C., Jakacki, J. 2008. On the importance of freshwater fluxes from the Arctic Ocean into the North Atlantic: the Nordic Seas versus Canadian Arctic Archipelago. Poster.

135. Meincke, J., Jonsson, S., Swift, J. H. 1992.Variability of convective conditions in the Greenland Sea. ICES Mar. Sci. Symp.195, 32–39.

136. Meincke, J., Rudels, B., Friedrich, H.J., 1997. The Arctic Ocean–Nordic Seas thermohaline system. ICES Journal of Marine Science, 54(3), pp.283-299.

137. Mironov E.U., Sea-ice conditions in the Greenland and Barents seas and their long-term preditions, 2004, St.Petersburg, AARI, 1-320 (In Russian).

138. Moore, G. W. K., Våge, K., Pickart, R. S., Renfrew, I. A. 2015. Decreasing intensity of open-ocean convection in the Greenland and Iceland seas. Nature Climate Change. 5, 877–882.

139. Moretsky V.N., Popov A.V. 1989. Water masses of the Norwegian and the Greenland seas and the principle types of vertical water structure in the region. Structure and variability of largescale processes in the Norwegian zone of intensive ocean-atmosphere interactions (eds. Nikolayev, Yu.V., Alekseev, G.V.). Hydrometeoizdat., Leningrad. 18-27. (In Russian)

140. Mulet, S., Rio, M.H., Mignot, A., Guinehut, S., Morrow, R., 2012. A new estimate of the global 3D geostrophic ocean circulation based on satellite data and in-situ measurements. Deep Sea Research II, 77, 70-81.

141. Muller, F. L., Wekerle, C., Dettmering, D., Passaro, M., Bosch, W., Seitz, F. (2019). Dynamic ocean topography of the northern Nordic seas: a comparison between satellite altimetry and ocean modelling. The Cryosphere, 13 (2).

142. Myers P. G., Josey S. A., Wheler B., Kulan N. 2007. Interdecadal variability in Labrador Sea precipitation minus evaporation and salinity. Progress in Oceanography. 73 (3-4), 341-357. https://doi.org/10.1016/j.pocean.2006.06.003

143. Mysak, L. A., Manak, D. K., Marsden, R. F. 1990. Sea ice anomalies observed in the Greenland and Labrador Seas during 1901–1984 and their relation to an interdecadal Arctic climate cycle. Climate Dynamics. 5 (2), 111-133.

144. Nagurny. A. P. Popov, A. V. 1985. Intensive upwelling of deep and bottom waters and their formation at the surface in the region of the Greenland Hollow. Meteorologiyai Gidrologya. 7, 71-75. (In Russian)

145. Nansen F. 1912. Das Bodenwasser und die Abkühlung des Meeres. Int. Rev. Hydrobiol. 5, 1–42.

146. Nikolayev, Yu.V., Alekseev, G.V. (eds.) 1989. Structure and variability of largescale processes in the Norwegian zone of intensive ocean-atmosphere interactions. Hydrometeoizdat., Leningrad. pp.124. (In Russian)

147. Nurser, A.J.G., Bacon, S., 2014. The Rossby radius in the Arctic Ocean. Ocean Science, 10(6), pp.967-975.

148. Paluszkiewicz, T., Romea, R. D. 1997. A one-dimensional model for the parameterization of deep convection in the ocean. Dynamics of Atmospheres and Oceans, 26(2), 95–130. https://doi.org/10.1016/S0377-0265(96)00482-4

149. Peterson B. J., McClell J., Curry R., Holmes R. M., Walsh J. E., Aagaard K. 2006. Trajectory shifts in the Arctic and subarctic freshwater cycle. Science. 313 (5790), 1061-1066. doi: 10.1126/science.1122593.

150. Piechura, J., Walczowski, W. (2009). Warming of the West Spitsbergen Current and sea ice north of Svalbard. Oceanologia, 51(2), 147–164. https://doi.org/10.5697/oc.51-2.147

151. Pickart, R.S., Torres, D.J., Clarke, R.A. 2002. Hydrography of the Labrador Sea during active convection. J. Phys. Oceanogr. 32, 428–457. https://doi.org/10.1175/1520-0485(2002)032<0428:HOTLSD>2.0.CO;2

152. Proshutinsky, A., Dukhovskoy, D., Timmermans, M. L., Krishfield, R., Bamber, J. L. 2015.Arctic circulation regimes. Phil. Trans. R. Soc. A. 373 (2015), 20140160.https://doi.org/10.1098/rsta.2014.0160

153. Rabe, B., Dodd, P. A., Hansen, E., Falck, E., Schauer, U., Mackensen, A., ... Cox, K. 2013. Liquid export of Arctic freshwater components through the Fram Strait 1998–2011. Ocean Science. 9 (1), 91-109. doi:10.5194/os-9-91-2013

154. Rahmstorf, S., Box, J. E., Feulner, G., Mann, M. E., Robinson, A., Rutherford, S., Schaffernicht,E. J. 2015. Exceptional twentieth-century slowdown in Atlantic Ocean overturning circulation. Nat. Clim. Change. 5*(*5*)*, 475–480. *doi:*10.1038/nclimate2554.

155. Raj, R. P., Nilsen, J. Ø., Johannessen, J. A., Furevik, T., Andersen, O. B., Bertino, L. (2018). Quantifying Atlantic Water transport to the Nordic Seas by remote sensing. Remote Sensing of Environment, 216, 758-769.

156. Rasmussen, E., Turner, J. 2003. Polar Lows: Mesoscale Weather Systems in the Polar Regions. Cambridge University Press. 612 pp.

157. Renold, M., Raible, C. C., Yoshimori, M., and Stocker, T. F. 2010. Simulated resumption of the North Atlantic meridional overturning circulation–Slow basin-wide advection and abrupt local convection. Quaternary Science Reviews, 29(1-2), 101-112.

158. Rhein, M. 1996. Convection in the Greenland Sea, 1982–1993. Journal of Geophysical Research: Oceans. 101 (C8), 18183-18192. doi:10.1029/96JC01295.

159. Rhein, M., Kieke, D., Hüttl-Kabus, S., Roessler, A., Mertens, C., Meissner, R., ... Yashayaev, I. 2011. Deep water formation, the subpolar gyre, and the meridional overturning circulation in the subpolar North Atlantic. Deep Sea Research Part II: Topical Studies in Oceanography, 58 (17), 1819-1832. https://doi.org/10.1016/j.dsr2.2010.10.061.

160. Ricker, R., Girard-Ardhuin, F., Krumpen, T. and Lique, C. (2018). Satellite-derived sea ice export and its impact on Arctic ice mass balance. The Cryosphere, 12(9), pp.3017-3032.

161. Ronski S., Budeus G., 2005. Time series of winter convection in the Greenland Sea, Journal of Geophysical Research: Oceans, 110, C04015, doi:10.1029/2004JC002318.

162. Rosmorduc, V., Hernandez, F. 2003. Two altimetric satellites minimum are needed for ocean observation and forecasting. AVISO Newsletter. 9, 12-14.

163. Rossby, T., Ozhigin, V., Ivshin, V. and Bacon, S., 2009. An isopycnal view of the Nordic Seas hydrography with focus on properties of the Lofoten Basin. Deep Sea Research Part I: Oceanographic Research Papers, 56(11), pp.1955-1971.

164. Rudels, B., Fahrbach, E., Meincke, J., Budéus, G. and Eriksson, P., 2002. The East Greenland Current and its contribution to the Denmark Strait overflow. ICES Journal of Marine Science, 59(6), pp.1133-1154.

165. Rudeva, I., Gulev, S. K. (2011). Composite analysis of North Atlantic extratropical cyclones in NCEP–NCAR reanalysis data. Monthly weather review, 139(5), 1419-1446.

166. Saberi A., Haine T. W., Gelderloos R., Femke de Jong M., Furey H., Bower A. 2020. Lagrangian Perspective on the Origins of Denmark Strait Overflow. Journal of Physical Oceanography, 50(8), 2393-2414

167. Schauer, U., Beszczynska-Möller, A., Walczowski, W., Fahrbach, E., Piechura, J., Hansen, E., 2008. Variation of measured heat flow through the Fram Strait between 1997–2006. In: Dickson, R.R., Meincke, J., Rhines, P. (Eds.), Arctic–Subarctic Ocean Fluxes. Springer, Dordrecht, pp. 65–85.

168. Schlosser, P., Bonisch, G., Rhein, M., Bayer, R. 1991. Reduction of deep water formation in the Greenland Sea during the 1980s: Evidence from tracer data. Science. 251 (4997), 1054-1056.

169. Schweiger, A., Lindsay, R., Zhang, J., Steele, M., Stern, H., and Kwok, R. 2011. Uncertainty in modeled Arctic sea ice volume. J. Geophys. Res. 116, C00D06. doi:10.1029/2011JC007084.

170. Selivanova, Yu.V., Tilinina, N. D., Gulev, S. K., Dobrolubov,S. A. 2016. An Impact of Sea Ice Cover on the Ocean–Atmosphere Turbulent Heat Fluxes in the Artic. Okeanologiya. 56 (1), 18–22. doi: 10.7868/S0030157416010184. (In Russian)

171. Selyuzhenok, V., Bashmachnikov, I, Ricker, R., Vesman, A., Bobylev, L., 2020. Sea ice volume variability and water temperature in the Greenland Sea. The Cryosphere, 14, 1–19, https://doi.org/10.5194/tc-14-477-2020

172. Serreze, M. C., Barrett, A. P., Slater, A. G., Woodgate, R. A., Aagaard, K., Lammers, R. B., ... Lee, C. M. 2006. The large-scale freshwater cycle of the Arctic. Journal of Geophysical Research: Oceans. 111, C11010. doi:10.1029/2005JC003424.

173. Smirnova, J.E., Golubkin, P.A., Bobylev, L.P., Zabolotskikh, E.V., Chapron, B.. 2015. Polar low climatology over the Nordic and Barents seas based on satellite passive microwave data. Geophysical Research Letters. 42(13), pp.5603-5609.

174. Smirnova, J., Golubkin, P. 2017. Comparing polar lows in atmospheric reanalyses: Arctic System Reanalysis versus ERA-Interim. Monthly Weather Review. 145(6), pp.2375-2383.

175. Somavilla, R. 2019. Draining and upwelling of Greenland Sea deep waters. Journal of Geophysical Research: Oceans, 124, 2842– 2860. https://doi.org/10.1029/2018JC014249

176. Srokosz, M., Baringer, M., Bryden, H., Cunningham, S., Delworth, T., Lozier, S., ..., Sutton, R. (2012). Past, present, and future changes in the Atlantic meridional overturning circulation. Bulletin of the American Meteorological Society, 93(11), 1663-1676.

177. Shalina, E. V., & Sandven, S. (2018). Snow depth on Arctic sea ice from historical in situ data. The Cryosphere, 12(6), 1867-1886.

178. Stommel, H. 1958. The abyssal circulation. Deep Sea Research, 5, 80–82.

179. Swingedouw, D., Rodehacke, C.B., Olsen, S.M., Menary, M., Gao, Y., Mikolajewicz, U., Mignot, J., 2014. Impact of Greenland ice sheet melting on the Atlantic overturning: A multi-model assessment. Climate Dynamics. 44 (11–12), 3261–3279. doi 10.1007/s00382-014-2270-x

180. Thomson, R.E., Emery, W.J. 2014. Data analysis methods in physical oceanography. Third edition, Elsevier, Amsterdam, 1-716.

181. Tilinina, N.D., Gulev, S.K. and Gavrikov, A.V., 2016. Formation of extreme surface turbulent heat fluxes from the ocean to the atmosphere in the North Atlantic. Oceanology, 56(1),1-5.

182. Timmermann, R., Beckmann, A. 2004. Parameterization of vertical mixing in the Weddell Sea. Ocean Modelling, 6(1), 83–100. https://doi.org/10.1016/S1463-5003(02)00061-6

183. Trodahl, M. Isachsen, P.E. 2018. Topographic Influence on Baroclinic Instability and the Mesoscale Eddy Field in the Northern North Atlantic Ocean and the Nordic Seas.J. Phys. Oceanogr.48, 2593–2607. https://doi.org/10.1175/JPO-D-17-0220.1.

184. Våge, K., Pickart, R. S., Spall, M. A., Moore, G. W. K., Valdimarsson, H., Torres, D. J., ..., Nilsen, J. E. Ø. 2013. Revised circulation scheme north of the Denmark Strait. Deep Sea Research Part I: Oceanographic Research Papers, 79, 20-39.

185. Våge, K., Papritz, L., Håvik, L., Spall, M.A. and Moore, G.W.K., 2018. Ocean convection linked to the recent ice edge retreat along east Greenland. Nature communications, 9(1), p.1287

186. Walczowski, W. 2014. Atlantic Water in the Nordic Seas: Properties, Variability, Climatic Importance, GeoPlanet Earth Planet. Sci., 13, doi:10.1007/978-3-319-01279-7.

187. Verbrugge, N., Mulet, S., Guinehut, S., 2017. Quality Information Document for Global Ocean Observation-based Products, GLOBAL_ANALYSIS_PHYS_001_020.

188. Vesman, A. V., Bashmachnikov, I. L., Golubkin, P. A., Raj, R. P. 2020. The coherence of the oceanic heat transport through the Nordic seas: oceanic heat budget and interannual variability. Ocean Science Discussions, 1-24.
189. Vessey, A.F., Hodges, K.I., Shaffrey, L.C., Day, J.J. 2020. An inter-comparison of Arctic synoptic scale storms between four global reanalysis datasets. Climate Dynamics. 54, 2777–2795.
190. Vinje T., Finnekasa O. 1986. The ice transport through the Fram strait. Norsk Polarinstitutt, Oslo. 186 (40).
191. Visbeck, M., Marshall, J., Jones, H. 1996. Dynamics of Isolated Convective Regions in the Ocean. Journal of Physical Oceanography, 26, 1721–1734. https://journals.ametsoc.org/view/journals/phoc/26/9/1520-0485_1996_026_1721_doicri_2_0_co_2.xml
192. Volkov, D.L., Meinen, C. S., Schmid, C., Moat, B., Lankhorst, M., Dong, S., ..., Goni, G. 2020. Atlantic meridional overturning circulation and associated heat transport. In: Blunden, J.; Arndt, D. S., (eds.) State of the climate in 2019. Bulletin of the American Meteorological Society, 101(8), 159-163, doi: 10.1175/BAMS-D-20-0105.1
193. von Appen, W. J., Wekerle, C., Hehemann, L., Schourup-Kristensen, V., Konrad, C., Iversen, M. H. (2018). Observations of a submesoscale cyclonic filament in the marginal ice zone. Geophysical Research Letters, 45(12), 6141-6149.
194. Wadhams, P., Budéus, G., Wilkinson, J. P., Løyning, T., Pavlov, V. (2004). The multi-year development of long-lived convective chimneys in the Greenland Sea. Geophysical research letters, 31(6), L06306, doi:10.1029/2003GL019017.
195. Whitehead J.A. (2000): Stratified convection with multiple states. Ocean Modelling, 2, 109-121.
196. Yang, Q., Dixon, T. H., Myers, P. G., Bonin, J., Chambers, D., Van Den Broeke, M. R. 2016. Recent increases in Arctic freshwater flux affects Labrador Sea convection and Atlantic overturning circulation. Nature communications, 7, 10525.
197. Yashayaev, I. 2007. Hydrographic changes in the Labrador Sea, 1960–2005. Prog. Oceanogr. 73, 242–276. https://doi.org/10.1016/j.pocean.2007.04.015.
198. Yashayaev I., 2011. Deep water formation, the subpolar gyre, and the meridional overturning circulation in the subpolar North Atlantic, Deep Sea Res. Part II, 58 (17), 1819-1832
199. Yashayaev, I., Seidov, D., 2015. The role of the Atlantic Water in multidecadal ocean variability in the Nordic and Barents Seas. Progress in oceanography, 132, pp.68-127.
200. Zhang J. L. Rothrock D. A. 2003. Modeling global sea ice with a thickness and enthalpy distribution model in generalized curvilinear coordinates. Monthly Weather Review, 131, 845-861, https://journals.ametsoc.org/view/journals/mwre/131/5/1520-0493_2003_131_0845_mgsiwa_2.0.co_2.xml .
201. Zolina, O., Gulev, S.K. 2003. Synoptic variability of ocean-atmosphere turbulent fluxes associated with atmospheric cyclones. Journal of climate. 16, 2717-2734. https://journals.ametsoc.org/view/journals/clim/16/16/1520-0442_2003_016_2717_svootf_2.0.co_2.xml.
202. Zhang, J., Rothrock, D. A. 2003. Modelling global sea ice with a thickness and enthalpy distribution model in generalized curvilinear coordinates. Monthly Weather Review, 131 (5), 845-861.
203. Zhang, J., Steele, M., Rothrock, D. A., Lindsay, R. W. (2004). Increasing exchanges at Greenland-Scotland Ridge and their links with the North Atlantic Oscillation and Arctic sea ice. Geophysical Research Letters, 31(9), 1-5, doi: 10.1029/2003GL019304.